

Article

Geomorphological Geometries and High-Resolution Seismic Sequence Stratigraphy of Malay Basin's Fluvial Succession

Abd Al-Salam Al-Masgari ^{1,2,*}, Mohamed Elsaadany ¹, Numair A. Siddiqui ¹, Abdul Halim Abdul Latiff ¹ , Azli Abu Bakar ¹, Sami Elkurdy ¹, Maman Hermana ¹ , Ismailalwali Babikir ¹, Qazi Sohail Imran ¹ and Teslim Adeleke ¹

¹ Centre for Subsurface Imaging, Department of Geosciences, Universiti Teknologi PETRONAS, Bandar Seri Iskandar, Tornoh 32610, Malaysia; mohamed.elsaadany@utp.edu.my (M.E.); numair.siddiqui@utp.edu.my (N.A.S.); abdulhalim.alatiff@utp.edu.my (A.H.A.L.); azli_abubakar@petronas.com (A.A.B.); selkurdy@gmail.com (S.E.); maman.hermana@utp.edu.my (M.H.); ismailalwal_19001505@utp.edu.my (I.B.); qazi_17007588@utp.edu.my (Q.S.I.); teslim-180003571@utp.edu.my (T.A.)

² Department of Geology and Environment, Faculty of Applied Science, Thamar University, Dhamar 124401, Yemen

* Correspondence: almasgari@gmail.com

Abstract: This study identified the Pleistocene depositional succession of the group (A) (marine, estuarine, and fluvial depositional systems) of the Melor and Inas fields in the central Malay Basin from the seafloor to approximately -507 ms (522 m). During the last few years, hydrocarbon exploration in Malay Basin has moved to focus on stratigraphic traps, specifically those that existed with channel sands. These traps motivate carrying out this research to image and locate these kinds of traps. It can be difficult to determine if closely spaced-out channels and channel belts exist within several seismic sequences in map-view with proper seismic sequence geomorphic elements and stratigraphic surfaces seismic cross lines, or probably reinforce the auto-cyclic aggregational stacking of the avulsing rivers precisely. This analysis overcomes this challenge by combining well-log with three-dimensional (3D) seismic data to resolve the deposition stratigraphic discontinuities' considerable resolution. Three-dimensional (3D) seismic volume and high-resolution two-dimensional (2D) seismic sections with several wells were utilized. A high-resolution seismic sequence stratigraphy framework of three main seismic sequences (3rd order), four Parasequences sets (4th order), and seven Parasequences (5th order) have been established. The time slice images at consecutive two-way times display single meandering channels ranging in width from 170 to 900 m. Moreover, other geomorphological elements have been perfectly imaged, elements such as interfluves, incised valleys, chute cutoff, point bars, and extinction surfaces, providing proof of rapid growth and transformation of deposits. The high-resolution 2D sections with Cosine of Phase seismic attributes have facilitated identifying the reflection terminations against the stratigraphic amplitude. Several continuous and discontinuous channels, fluvial point bars, and marine sediments through the sequence stratigraphic framework have been addressed. The whole series reveals that almost all fluvial systems lay in the valleys at each depositional sequence's bottom bars. The degradational stacking patterns are characterized by the fluvial channels with no evidence of fluvial aggradation. Moreover, the aggradation stage is restricted to marine sedimentation incursions. The 3D description of these deposits permits distinguishing seismic facies of the abandoned mud channel and the sand point bar deposits. The continuous meandering channel, which is filled by muddy deposits, may function as horizontal muddy barriers or baffles that might isolate the reservoir body into separate storage containers. The 3rd, 4th, and 5th orders of the seismic sequences were established for the studied succession. The essential geomorphological elements have been imaged utilizing several seismic attributes.

Keywords: seismic sequence stratigraphy; geomorphic geometries; fluvial deltaic; seismic facies; Malay Basin



Citation: Al-Masgari, A.A.-S.; Elsaadany, M.; Siddiqui, N.A.; Latiff, A.H.A.; Bakar, A.A.; Elkurdy, S.; Hermana, M.; Babikir, I.; Imran, Q.S.; Adeleke, T. Geomorphological Geometries and High-Resolution Seismic Sequence Stratigraphy of Malay Basin's Fluvial Succession. *Appl. Sci.* **2021**, *11*, 5156. <https://doi.org/10.3390/app11115156>

Academic Editor: Edoardo Rotigliano

Received: 16 March 2021

Accepted: 29 March 2021

Published: 2 June 2021

Publisher's Note: MDPI stays neutral with regard to jurisdictional claims in published maps and institutional affiliations.



Copyright: © 2021 by the authors. Licensee MDPI, Basel, Switzerland. This article is an open access article distributed under the terms and conditions of the Creative Commons Attribution (CC BY) license (<https://creativecommons.org/licenses/by/4.0/>).

1. Introduction

Significant development of the three-dimensional (3D) seismic data acquisition over the past few decades has been achieved. Data processing, hydrocarbon exploration analyses, and seismic geomorphology is now a critical method for understanding a wide variety of depositional settings from shore to sea environments. This includes shallow marine settings of shelf deltas, cliffs, and submarine deep-sea fans' settings [1–13]. The researchers have demonstrated that the 3D seismic data enables identifying distinct geomorphological features. However, there is low vertical resolution in 3D seismic data to distinguish sedimentary and stratigraphic elements that are discontinuous in the sub-surface's seismic section. It is essential to delineate sequence stratigraphic unconformities and discontinuous reflections to establish a hierarchy chronology and genetically distinguish diverse geomorphic entities visualized in map surfaces (such as various fluvial channels and their channel belts) [14]. The traditional seismic 3D data can be complicated with no such surfaces and chronologically distinguishing closely spaced geomorphologic elements. The conventional 3D seismic interpretation is incapable of delineating stratigraphic discontinuities due to this technique's primary limitation in the Malay Basin [15].

Consequently, it is challenging to compare geomorphic elements truthfully and precisely in map-view with precise seismic sequence-stratigraphic surfaces in seismic cross lines. Whichever closely spaced-out channels and channel belts exist within several seismic sequences or probably reinforce auto-cyclic aggregational stacking of the avulsing rivers can be challenging to determine. This research overcomes this obstacle by incorporating the 3D seismic data with a well log to approach the considerable resolution of depositions' stratigraphic discontinuities. With roughly 25 times the higher vertical resolution than the 3D seismic volume, two-dimensional (2D) data provide a resolution of about 25 cm and enable a comprehensive stratigraphic framework identification. Therefore, erosional stratigraphic discontinuities with high amplitude can be interpreted on the seismic volume compared with geomorphic elements visualized in 3D seismic data [16].

The Malay Basin is a Tertiary trans-tensional rift basin situated in offshore Peninsular Malaysia [17]. The basin trends north-west/south-east and covers an area of about 80,000 square kilometers. It contains over 12 km or more Oligocene to recent sediments. The basin is adjacent to the Penyau and West Natuna basins to the south and south-east (Figure 1) [18,19]. The Tenggol Arch separates the Malay Basin from the Penyau Basin (Figure 1), while the Narathiwat High separates the Malay Basin from Thailand's Patani Basin.

The Inas and Melor fields are considered gas fields located in block PM 313, roughly 215 km north-northeast of Kertih, Terengganu, and 70 km northeast of the Resak production platform. The data used in this research comprises an area of roughly 574 square kilometers in the Malay Basin. The alternation of the marine and fluvial sediments in the uppermost deposited succession –507 ms of the Malay Basin shows submergence and shelf exposure several times through the Pleistocene [20,21]. Some factors include the sea-level changes, climate, and sediment supply that probably share control of the accommodation space and, consequently, the basin fill geometry [2].

Three fluvial sequences were established at various depths in the 3D seismic data and laterally in the 2D seismic cross-sections. Earlier researchers [18] proposed that this section's topmost layer is lower Pliocene to Quaternary in age (Figure 2). The continental scale's fluvial system has been imaged using the available seismic volume and well logs with the current Chao Phraya River's exact trajectory that passes via Bangkok and into the Thailand Gulf. This river ranges from 150 m to around 230 m, and is around 50 km long from the land to the shoreline [22,23]. The evaluated succession covers the topmost –507 ms (522–550 Measured Total Vertical Depth Subsea (MTVDSS)) underneath sea level, as shown in Figure 3, which was previously labeled as Group A by Ibrahim and Madon, 1990 [24].

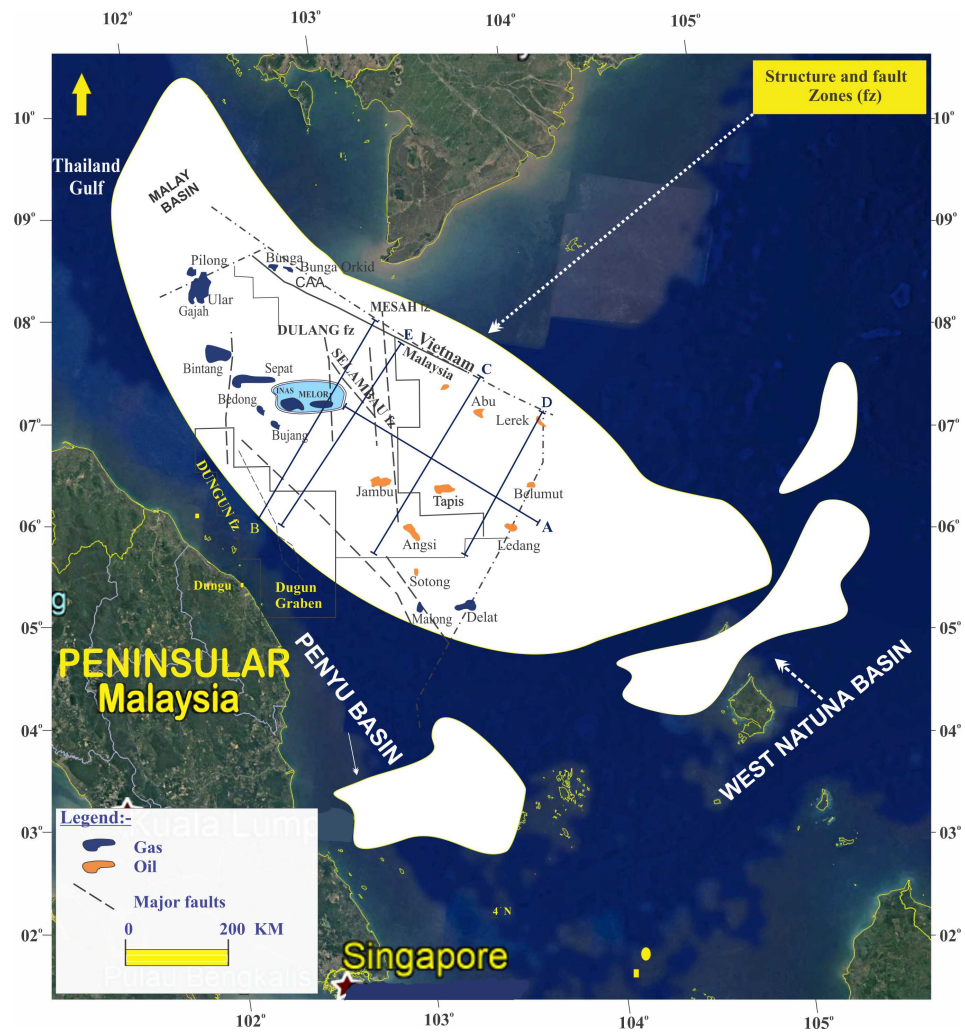


Figure 1. The map of the study area Malay Basin was modified and retraced after Madon (1999) [17].

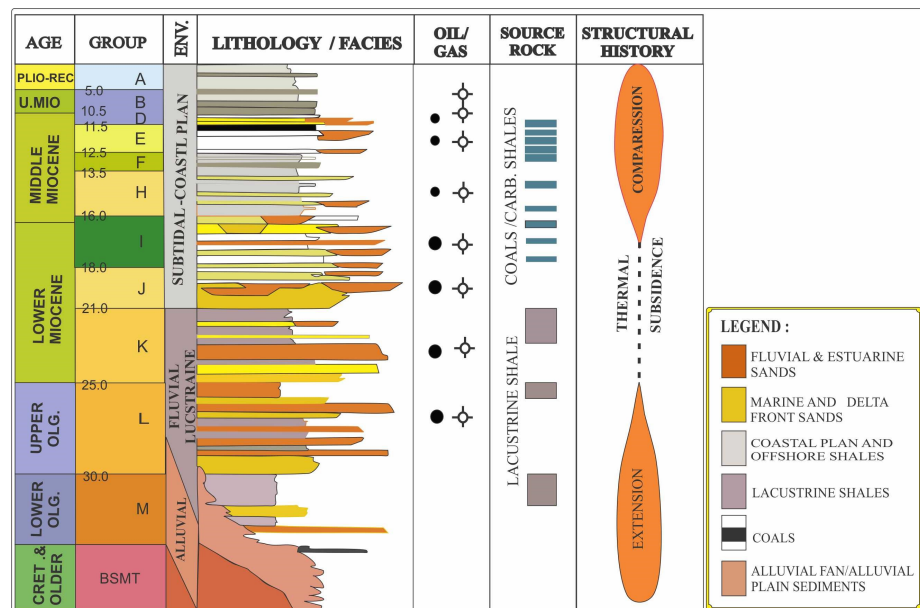


Figure 2. A layout shows the generalized stratigraphy and structural, historical column of the Malay Basin. The second column contains the main column of the successions of geographic stratigraphy and their approximate ages (categorized A–M) (in Mya), in addition to the dominant lithologies and possible associated facies, after Madon (1999) [17].

Some previous investigations have implemented a regional study of the Malay basin's petroleum system [18]. The transgressive and regressive cycles in the Malay Basin have been investigated [25]. Moreover, the evolution of a Late Pleistocene incised valley, facies architecture, and analyzing recent fluvial point-bar deposits have been addressed as well, using regional seismic data, from References [1,26]. These studies are typically limited regarding the resolution achieved, representing only a regional investigation. However, this investigation can be considered the first integrated research in this area. This study gathers detailed analyses of the facies construction of fluvial deltaic systems and estuarine deposits utilizing the high-resolution 2D seismic sections, new seismic attributes, and time slices. The geomorphic features within the 3D seismic data have been extracted.

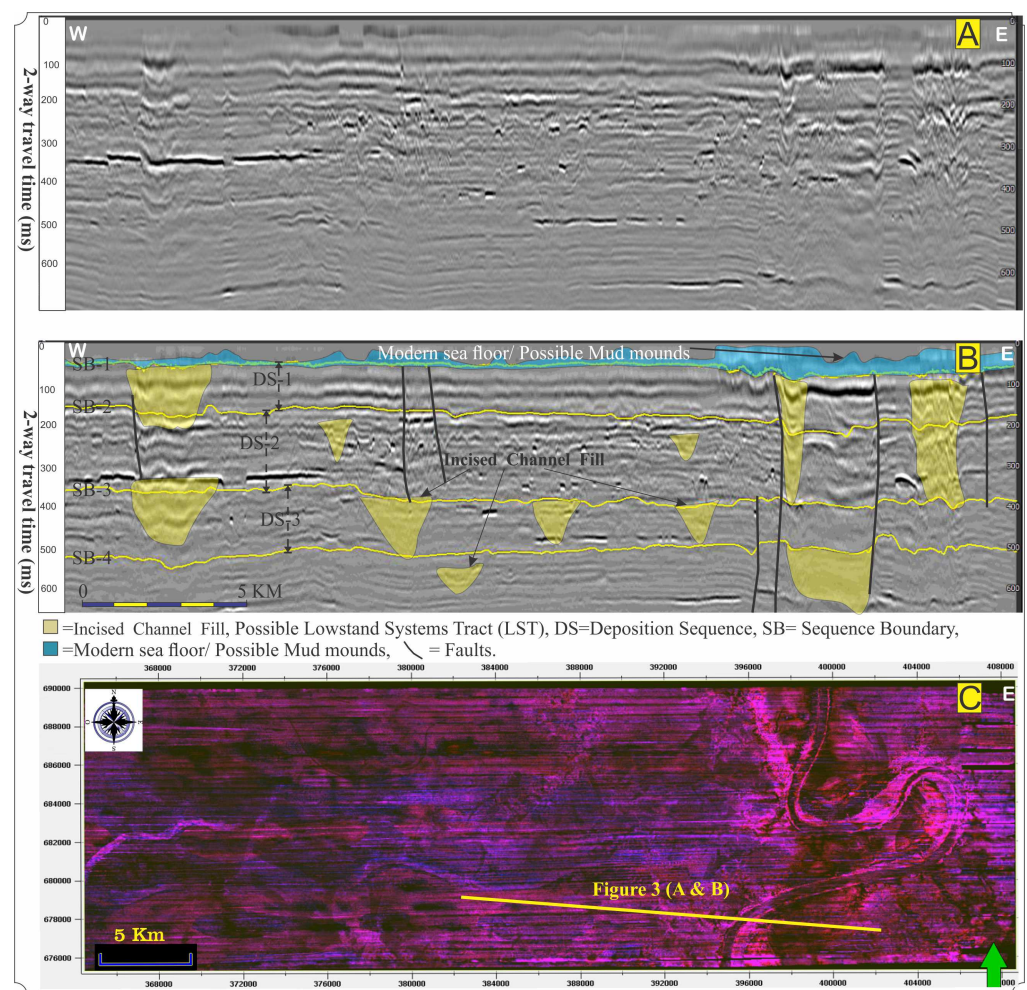


Figure 3. (A) The noninterpreted and (B) interpreted two-dimensional (2D) high-resolution seismic sections representing three major depositional sequence stratigraphy units in the uppermost ~ 507 ms (522–550 MTVDSS), several depositional geometries are displayed in the 2D section and (C) a map-view of the studied fields show the shallowest fluvial channels and incised valleys.

Overall, other variables, such as fluctuations in the supply of sediments and fluvial discharges, dominated the accommodation space in the farthest upstream to the shoreline. Moreover, the accommodation space downstream near the shoreline was controlled by the sea level fluctuation [27]. However, the Sunda Shelf's low slope has likely facilitated quick and comprehensive transgressions and regressions, with only slight changes in the relative sea-level [28].

Due to the short period (Pleistocene) of the observed era succession, the tectonics factors are considered less significant influences. Implementation of sequence stratigraphic modeling was first based on marine seismic data [29] and later extended to cover the

continental deposits [30]. Several studies were applied with greater emphasis on deposition factors, including sediment influx, climate, sea-level changes, subsidence, and tectonic control [31–36]. The model has been utilized in this investigation to understand the sedimentary fill evolution better and estimate the geomorphological elements of the deposited succession.

Existing incised valley models necessitate multistory fluvial strata as an essential identification criterion [21,35,37]. Such valley models propose that multistory filled valleys might not even be a necessity to describe such incised valley. For instance, such incised valley may have an effective twisting river sitting on its bottom throughout a lower sea level. If the correct physiographic and accommodation requirements are fulfilled through the transgression cycle, the valley may encounter sudden flooding, resulting in an immediate backstepping of the valley's coastline and fluvial network flooding [38]. The resulting filled canyon might not display an aggregational multistory canyon fill, as expected in References [39,40]. Rather than being characterized by a single sedimentary fluvial story at the canyon's bottom, it is defined by estuarine and/or open-sea mudstones, as clarified in this review overlain by estuarine and/or open-sea mudstones [38].

The study objectives can be surmised in several points: (1) Interpretation of the seismic sequence stratigraphic in the topmost studied succession, roughly -507 ms (522–550) True Vertical Depth SS (MTVDSS) from the seafloor. Furthermore, assessing the interpreted units' corresponding system tracts. (2) Describe the study area's main deposition processes and identify the seismic facies nature of the deltaic deposits. (3) Offer a comprehensive seismic geomorphologic analysis of the studied succession through depicting the stratigraphic features with the fluvial deltaic's geomorphologic elements. (4) Characterize the discontinuity in stratigraphy within the 2D seismic sections to distinguish the genetically different fluvial characteristics found in 3D time slices, thus enabling the geomorphic characteristics correlation with bed-scale stratigraphy, and (5) establish the morphological framework of the channel and channel belt and reveal the distribution of the sand and mud within such coastal environments.

2. Data and Methodology

A cube of raw 3D seismic data acquired and cropped for Inas and Melor fields was used in this study, which is located in the PM 313 block. The Inas and Melor 3D seismic survey covers an area of approximately 574 square kilometers. The data consists of 600 in-lines in the East–West directions and 3538 crosslines in the North–South direction. Data were recorded at a sampling rate of 2 milliseconds to 6.5 s of record length, with a line spacing of 25 m, while the Common Depth Point (CDP) spacing is 12.5 m, in-line length is 44,212.25 m, and the crossline length is about 14,975 m.

Using the Pre-Stack Time Migration (PrSTM) data, including full-fold, near, far seismic cubes with reverse SEG-Y polarity, the data were resampled to 3 runs during the processing chain to expedite data delivery. Data quality is relatively good in the zone of interest (Groups A), with a dominant frequency of about 67 Hz, which occurs in the time interval starting from 0 to -507 milliseconds. The minimum resolution is estimated at 25 m at the study succession. The seismic (16-bits SEG-Y) data (The SEG-Y (sometimes SEG Y) file format is one of several standards developed by the Society of Exploration Geophysicists (SEG) for storing geophysical data. It is an open standard, and is controlled by the SEG Technical Standards Committee, a non-profit organization) volume was loaded into Petrel 2019, Paleoscan 2019 to delineate the surfaces and boundaries.

Generally, both horizontal and vertical resolutions depend on similar data, reliant on different factors (velocity, wavelength, frequency, and noise). Some of the observable depositional features such as scroll bars in any point bar are simpler to image, recognize, and then interpret in the perspective of the 3D map-view. However, the same geological features can be depicted in a perspective view of the seismic cross-section, but in low detail compared to the 3D map view. Commonly, inferring a geological description from a view

of the plan is more manageable than from an image view of the section. The workflow followed in this research is summarized in Figure 4.

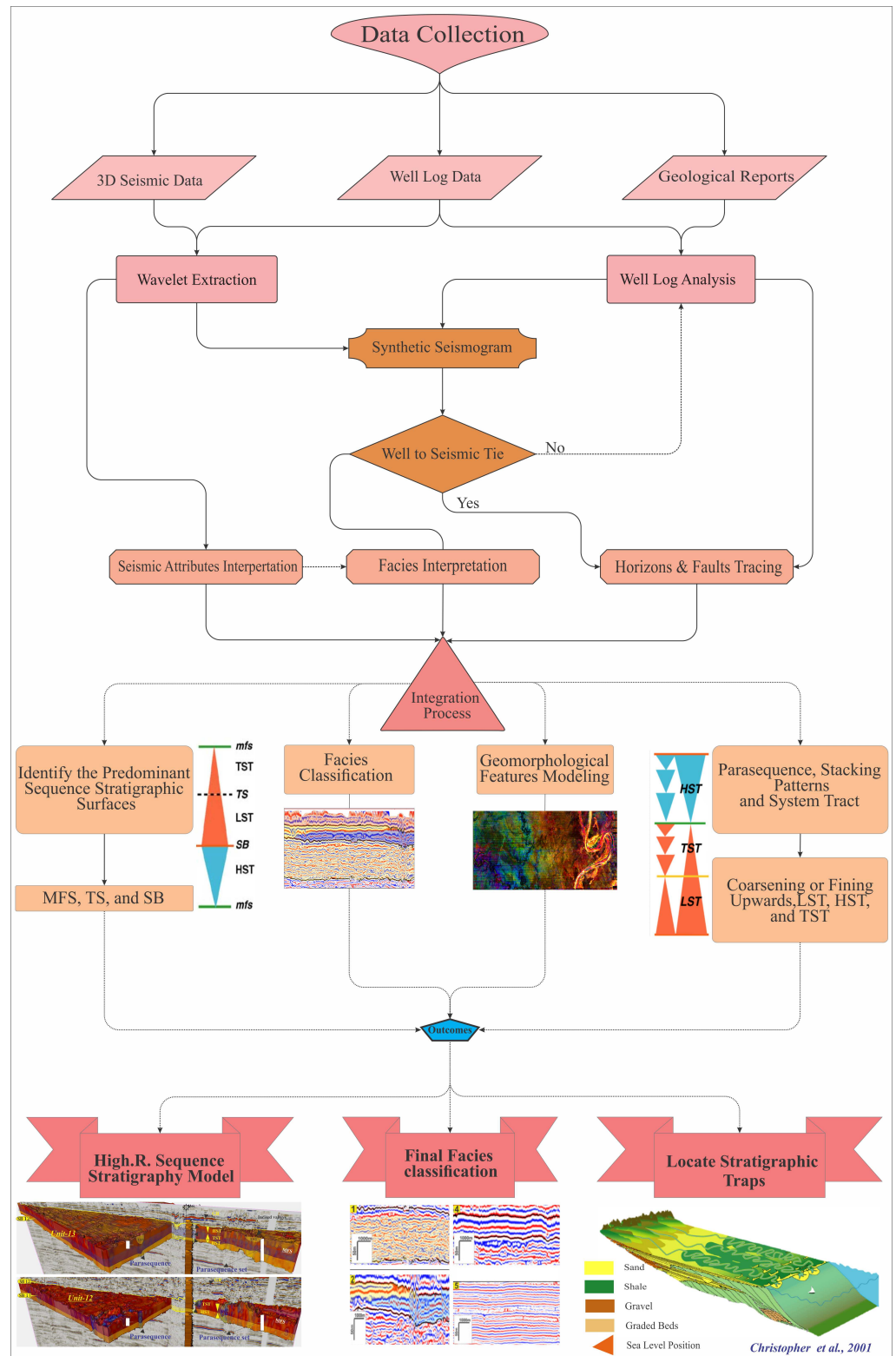


Figure 4. The general workflow for this research.

The strata slices' interpretations for such geomorphological evaluations provide a more accurate understanding of the lithology allocation and geologic system, such as stratigraphic analyses. The fluvial channel is an example where map-view elements might

include sinuosity channel, meander scrolls, laterally incised, and crevasse splays. These are all possibly measurable in slice pictures, especially compared to even more restricted information accessible in view of the seismic section [41]. The seismic section might describe some other attributes, including reservoir architecture and channel asymmetry. However, the range and abundance of information that can be found in sectional views are limited compared to what is accessible in time slices.

The optimal method, in general, should include incorporating observations from both views. However, time slices' images can facilitate and improve geological features' detection that cannot be identified using 2D seismic sections. The minimum thickness of strata to be detectable in seismic data is around 5.7 m [38]. Likewise, two different reflecting points in horizontal space must be roughly 11 m distance from each other to be observed as two different elements. Conversely, in this good condition set of data, which is close to the seafloor and consists of youthful deposits, geologic elements significantly smaller and laterally relatively close could even, therefore, be identified both in time slices and seismic crosslines.

A successful study of seismic geomorphology depends on the knowledge of sedimentological, geomorphological principles, understanding the local geological setting and seismic geomorphological imaging quality [12]. A conventional 3D seismic data interpretation method comprises cropped time slices at consecutive time values to detect and distinguish the development of geomorphic elements and structural directions in map views [7,42].

Seismic attribute maps exhibited at certain travel times can be categorized with shady colored points. The negative segments of the seismic wavelets are overlapped by the time slice, and bright colors where the positive sections of seismic wavelet are overlapped by the time slice [43]. The eventual results in shape-visualized time slices derived from the 3D seismic data have been evaluated to recognize geomorphologic elements in map-view, for example, seismic geomorphology features.

Few seismic attributes such as red-green-blue RGB color blending and spectral decomposition helped identify channel boundaries with limitations. Three different dominant iso-frequency values (15, 25, and 35 Hz) were utilized to generate the RGB color blending attribute. This attribute provided an excellent resolution of the channel geometries and channel boundaries, fill of channel, and inner thin bedding construction with thickness alteration of 10 to 15 m. In the studied successions, an average seismic velocity of 1500 m/s was used in the depth conversion. This velocity is an attribute of youthful inhomogeneous marine subsurface stratas, wealthy in sand and clay [44,45].

Overall, fifteen wells and their geological reports have been utilized to acquire the information of the sequence stratigraphic lithologies presented in the seismic sections. A modulation and framework were perfectly established for Group A by manipulating and integrating the 2D view and 3D visualization of the 3D seismic volume and well logs using Petrel 2019 and Paleoscan 2019 applications.

The internal reflection configurations have been employed to classify the typical seismic facies in the seismic volume. The seismic well tie tool allows integrated sonic calibration and synthetic generation within the well section window. The generated synthetic was utilized in turn to establish the sequence stratigraphy of the investigated succession. Moreover, the reflection terminations, seismic face variations, and well log information were used to establish sequence stratigraphy of the studied succession. All these factors have been utilized in the succession subdivision into the 3rd, 4th, and 5th orders.

This investigation offers the first incorporated study that integrates detailed deltaic deposition, seismic facies classification, sequence stratigraphy, and systems tract interpretation of the investigated succession.

3. Result and Discussion

Seismic Geomorphology Interpretation

A series of seismic volume time slices are shown in Figure 5, and Figure 6 reveals detailed main fluvial systems at different time intervals (−50, −68, −90, −111, −138, and −174 ms). A map-view of time slices is shown in Figure 5A,B, representing the beginning exposure of the channels at two different two-way times (−50 and −68 ms). However, the topmost exposure of the southwest meandering channel is shown in Figure 5(B-A), while Figure 5(B-B) reveals the topmost meandered channel's location at the east part of the studied area. Due to the nature of the study area deposits, which are generally sheet-like, the geomorphologic interpretation of time slices is working perfectly. Horizon slices (amplitude extractions simultaneous to trace the horizons) and flattened horizons function are especially effective for working with sloped or twisted rock layers.

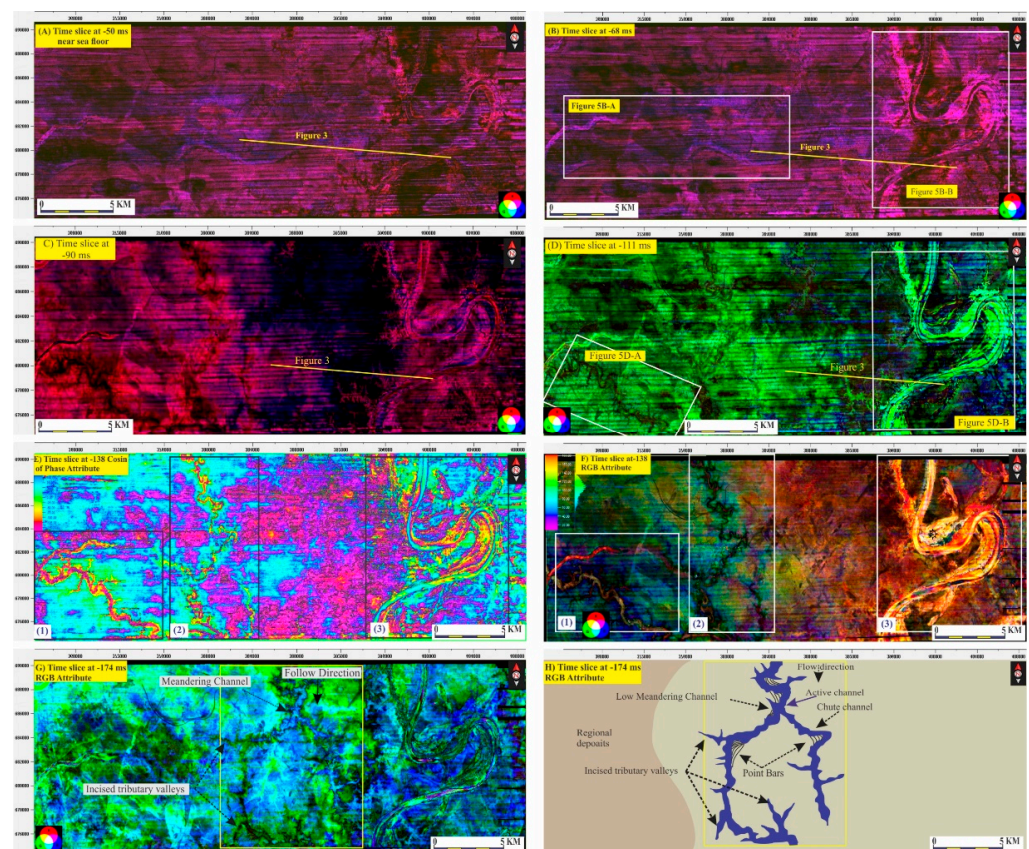


Figure 5. (A–H) Reveals the Melor and Inas fields' time slices at particular two-way times and covering an area of approximately 574 km². (A) Time slice of spectral decomposition attribute at −50 ms below the seafloor, (B) the time slice at −68 ms below the seafloor. (C) Time slice at −90 ms and the top major sinuous channel's uppermost features extending throughout the widespread channel belt in the right-side of the map-view with the other two minor channels in the left and south of the map-view. (D) The time slice at −111 ms exhibiting the major sinuous channel in the right side of the map view (Figure 5(D-B)) and a minor meandered channel with its tributaries in the southwest of the map view (Figure 5(D-A)). However, (E) shows time slice of the seismic Cosine of Phase attribute, revealing the time succession's fluvial channels system. (F) represent RGB color blending at −138 ms, exposing a continental meandering fluvial channel with paleo-flow trajectory from north to south. A minor sinuous channel is shown in the middle of the map-view. A medium sinuous channel is displayed with several tributaries at the southwest of the map view. (G) The time slice of the RGB color blending at −174 ms, displaying a continental low sinuous channel in the middle of the map-view with paleo-flow trajectory from north to south. (H) Explanation diagram highlighting the targeted channel with its tributaries and paleo-flow trajectory.

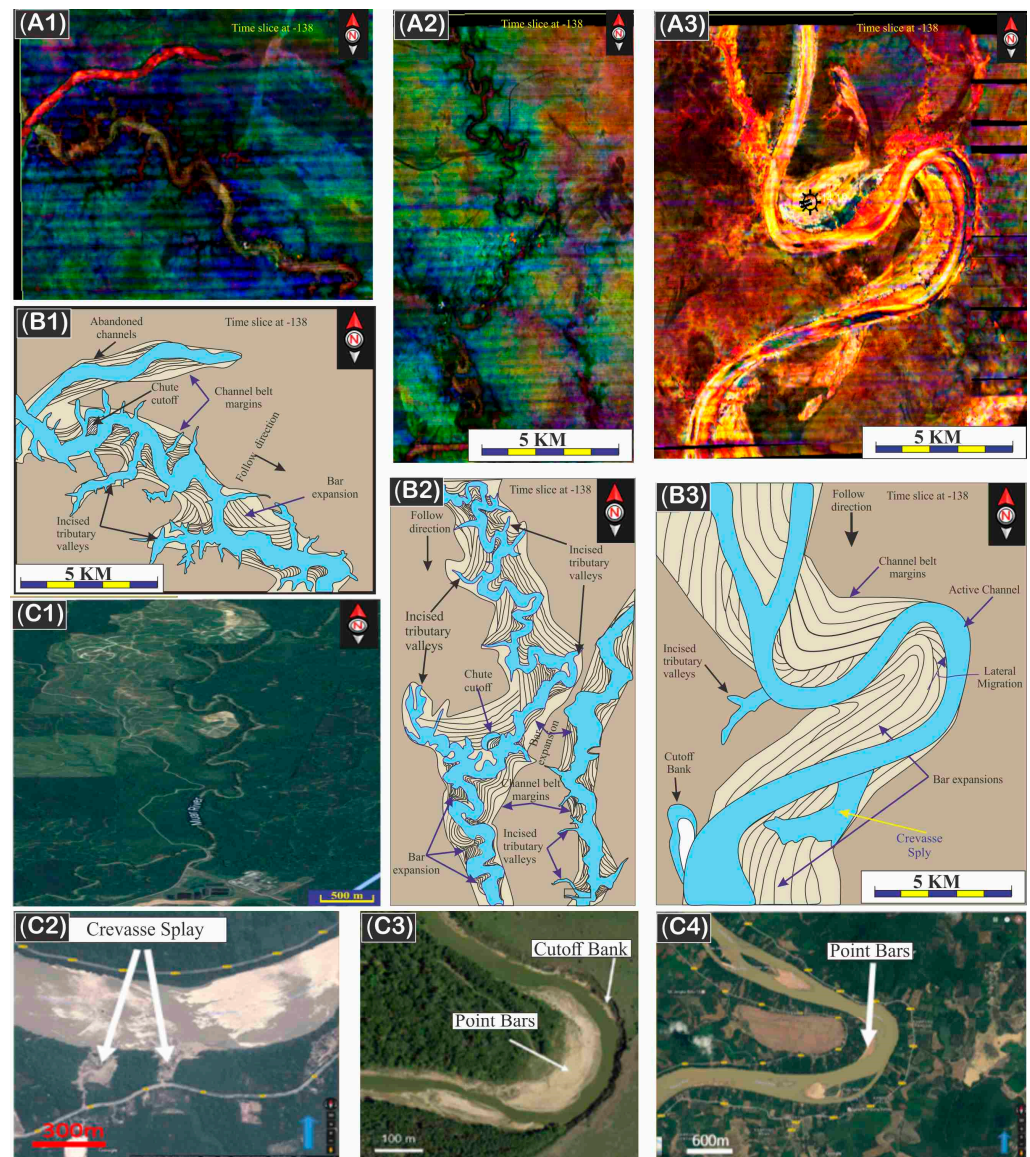


Figure 6. The map-view slides of continental channel belts and channels prominent at -138 ms. Slides (A1–A3) represent the time slices of RGB color blending seismic attribute at two way travel time (TWT) 138 ms, while (B1) shows a map-view representing the major geomorphological and depositional features of the southwest part of the studied area. Slide (B2) represents the meandering middle channels extended from the north to south, with the delineation of geomorphological elements. Slide (B3) shows the major sinuous channel at -138 ms. Satellite images in figures (C1–C4) reveal a recent analog with comparable features and similar depositional features, Muar River, Johor, Negeri Sembilan Pahang in Malaysia.

Figure 5A–H shows a series of seismic volume time slices at different two way travel time (TWT). Details of the main fluvial systems viewed at -50 , -68 , -90 , -111 , -138 , and -174 ms can be found in Figures 5 and 6. The sedimentary characteristics shown in Figure 5 have also been explained in the discussion part. A quick investigation (Figure 5A–H and Figure 6A1–C4) of the time slices display complicated views of grouped channels that appear to be overlaid on each other. These are map-views of channels and channel belts' directions that have been carefully spaced out in the vertical direction. This distribution makes it challenging to distinguish genetically different geomorphic characteristics in one 3D time slice. That is to say, 3D seismic slices cannot display the closely spaced geomorphic elements; therefore, they seem to exist on certain time slices, even though they are not

contemporary. A comprehensive description of the geomorphic elements situated on the top of the main stratigraphic discontinuities of the time slices at -90 , -111 , -138 , and -174 ms are shown in Figure 5A–H.

The 2D seismic sections were finally utilized to differentiate and identify multichannel systems. Correlation between channel belts and channels were visualized in cross-sectional channel fill pattern time slices (Figures 7 and 8). This correlation demonstrated that the fluvial systems shown in time slices are routinely focused beyond stratigraphic discontinuities in 2D lines (Figure 3). To image these geomorphic characteristics, 3D time slices were chosen to correspond to the principal stratigraphic discontinuities scale shown in Figure 3, as near as possible. Commonly, seismic time slices display lateral plans, which do not certainly follow the stratigraphic divergences' abnormal contours visible on 2D lines. Furthermore, this operation has shown that geomorphologic imaging on these surfaces has a reasonable estimation for accurate understanding and lineaments extraction.

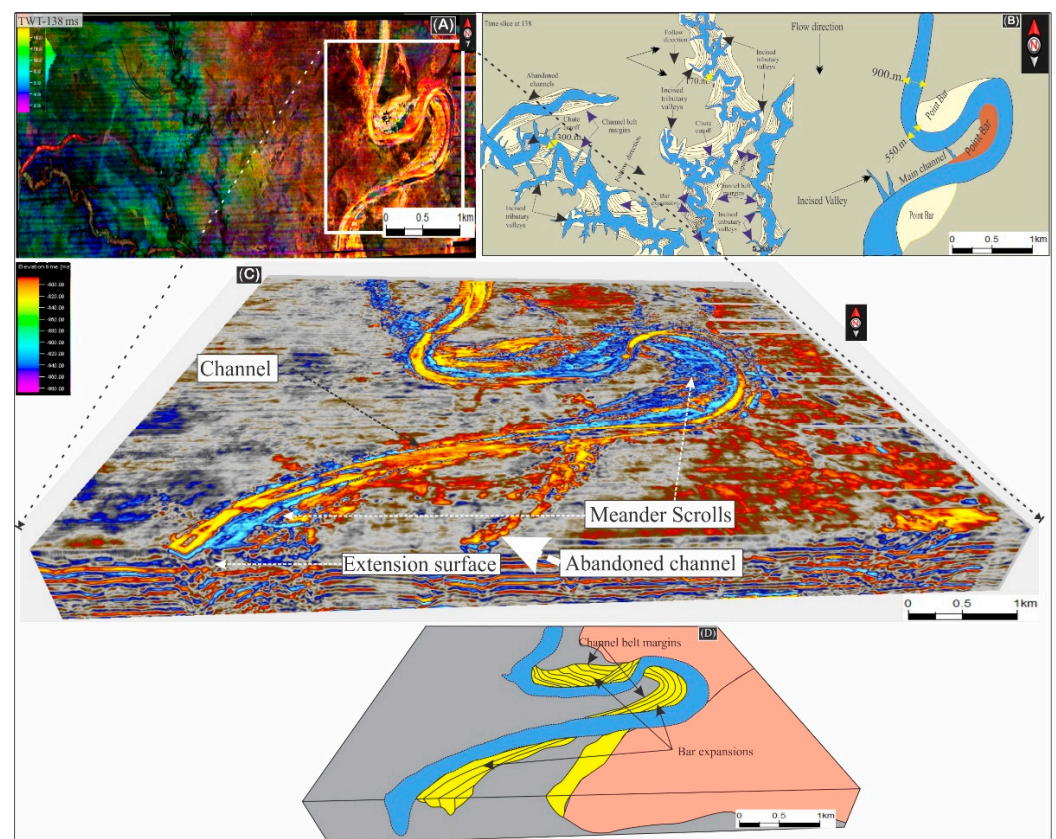


Figure 7. The block diagram illustrating the relationship between channel-fill shapes in the cross-sections and their chart-view interpretation was noticed at TWT of around -138 ms. (A) represents the RGB color blending seismic attribute at -138 . The time slice of chart view-imaged figure B represents well-conserved channel, and channel-belt muddy depositional features, highlighting the channel variation sizes shown in (B). The channel's seismic amplitude is quite different from the surrounded point bars deposits in both the 2D seismic sections and the 3D time slices, as shown in (C). The 3D amplitude volume reveals the biggest sinuosity channel crosses the Melor field; blue colors indicate the meander scrolls while the yellow color infers the sandy bodies filling the channel parts while others are filled with clay. However, (D)'s chart is an interpreted edition of the 3D seismic amplitude volume, displaying sand-prone facies in orange, mud-prone channel facies in blue, point bars in yellow interfluvial in gray and orange.

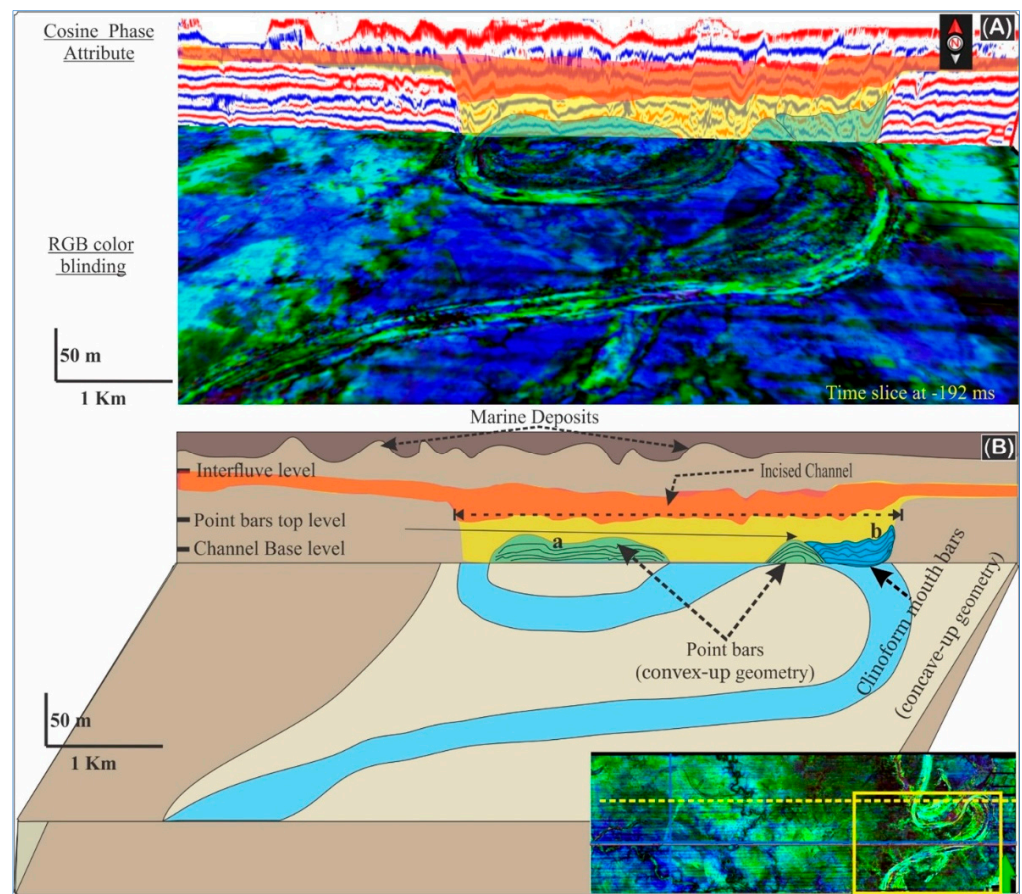


Figure 8. (A) chair display of the Cosine of Phase attribute cross-section with RGB seismic attribute time slice at 192 ms. Panel (B) represents the map view of the 2D seismic section showing the marine deposits, interfluvial, point bars, incised channel, and channel belts. A convex-up thick bed (Cyan) with horizontal reflections that formed down-laps on the channel walls. The point bars deposits were covered by transgressive deposits (Yellow). The uppermost deposits (Red) cover the entire valley and lay on the interfluvial topmost layer.

The geomorphologically interesting features imaged during rolling along the 3D seismic volume start from the seafloor and lie down on the new sea layers until about -507 ms (522 m) beneath sea level. A geological analysis of the drilled well was conducted in association with drilling activities. It is understood that these partly eroded deposits constitute fine clay sediments (mud mounds) associated with the current northwest-southeast sea-bottom, with sufficient speed from 2.5 to 3.5 m/s.

Evidence from Reference [38] in the investigation area indicates that these extended mounds contain erosion residues produced by the shallow marine source. The first reflection multiple of the seafloor depicting the geomorphic features at a certain level at about -50 ms below the surface are shown in the time slice view in Figure 5. Instantly beneath the seafloor, at -68 ms, two fluvial systems were defined in the southwest corner and eastern part, respectively, as shown in Figure 5(B-A,B-B).

A west-east trending low meandering channel with a narrow channel belt compared to the major channel belt on the other side at the southwest corner (Figure 5(B-A)) is shown at -68 ms, with slightly different colors of the west side and east side of the channel, which indicate variations in the imaged channel slope. Another highly meandering fluvial system channel extended from the north to south, and a bigger northwest-southeast direction channel belt with point-bars on both sides of the channel, are shown in the map-view, representing the major channel crossing the investigated fields (Figure 5(B-B)).

The geomorphological fluvial systems visualized at -90 ms (Figure 5C) are also categorized by three different paleo-flows, with north-south paleo-flow of the biggest

channel on the right side of the study area. This meandering feature, comparable in size and tortuosity to the current Chao Phraya River, displays a highly twisting sinuosity in the exhibited segment with scroll bars and point bars on both channel sides' meander loops. The other fluvial system is directed from north-west to south-east toward the south-southeast highly meandering channel, in the upstream, while the central segment exhibited a less-twisting zone, and an overlapped twisted channel in the downstream area.

The third feature detected was a low to medium sinuosity channel with narrow size and extended from west-southeast. At the TWT -111 ms, we also noticed a wider single fluvial channel in the right segment of the studied area extending from north to south, with a wider north-south meander channel belt gaining popularity along with the studied map (Figure 5(D-B)). Incisions categorize both the tortuous and the larger winding channels in the corresponding floodplains.

The time slice also displayed the base of the southwest channel (Figure 5(D-A)). The top of this channel was noticed at -90 ms with a small size and southwest direction. The depicted channel seems to be absent temporarily at -113 ms. The same channel is seen again when scrolling down through the seismic volume in the same area, but at -115 ms. However, the best shape is seen at -138 ms. This can be interpreted that a short transgression has taken place along the channel absence interval. A new progradation has taken place later, resulting in a new incision and forming the same channel's upper part. We noticed narrower-sized channels with some tributaries at this depth, and the meandering was also high compared with the map-view of the top of this channel.

The channel meandering at TWT -138 ms (Figures 5 and 6) shows the best example of conserved valley-fill and channel belt deposits in 2D seismic sections' 3D time slices. The Cosine of Phase and spectral decomposition attributes' time slices at -138 exhibit the biggest and obvious geomorphological fluvial systems, depicted as shown in Figures 5 and 6.

These continental tributaries are somewhat broader than the newer river Chao Phraya (Figure 6(C1)). This figure shows how different Cosine of Phase and RGB color attribute maps reveal geomorphic characteristics, such as point bars, channels, channel belts' margins, and tributary incised valleys, which is the way that the deposits in the fluvial trunk systems accumulate. The point bars and chute cutoffs have been imaged within the channel belts, demonstrating the transmission of the downstream and the bar expansion's meandering. The abandoned channel fills have various amplitudes responding from adjusting deposits in both Cosine of Phase and RGB color attributes, time slice maps, and cross-sections (Figure 8).

The time slice at TWT of -174 ms of RGB color blending of spectral decomposition attribute (Figure 5G,H) reveals an extended fluvial channel from north-south with low to moderate sinuosity, with a meander and narrow channel belt. A seismic artifact is shown in the right segment on the study area's map-view, and this artifact is due to a problem in seismic processing. This pseudo-channel is interpreted as a shadow of the above-observed channel at -138 ms. The main channel's low sinuosity reflects the substratum's higher slope, whereas the high sinuosity of channels indicates a lower depositional substratum slope. The degree of channel sinuosity can help in inferring the landscape slope during river flow. An abundance of incised tributary valleys develops along the channel at the southwest corner of the study area.

The channel shows more sinuosity on the west side and gets less towards the south direction, which is believed to be attributed to the river's pathway geomorphological gradient. At the center of this time slice, we noticed the top of the other high meandering channel extended from the north to south. On the right side of the study area is also a noticeable high sinuosity and meander channel extending from the north-south of the studied area's map-view with some incised tributary valleys. The incised tributary valleys are more visible and concentrate at the west side, while they are less whenever moving towards the downstream in the south direction.

This distinguishing feature is considered a result of the lateral lithological differences with assumed sand-laying flat facies associated with point bar sediments and muddy facies, resulting in a mud plug in the channel's last position before being abandoned. Besides, the major compression differences directly across the abandoned channels help define the mud-filled channel systems.

In the studied section, most fluvial systems were formed of one-channel zigzagging rivers, which vary widely from less than 100 to 900 m wide (Figure 7). Some minor fluvial systems are tiny and therefore do not display channel belts and bar sediments. The meandering fluvial systems at the TWT of -90 , -111 , -138 , and -174 ms have shown clearly evolved channel belts with widths up to 6 km. The above components are slightly bigger than the Muar River's present shape, which passes through the states of Johor, Negeri Sembilan, and Pahang in Malaysia, and is significant compared with other mainland analogs, like river Ucayali in Peru (Figure 6C1).

The southwestern segment of the trunk valley displays well-photographed carved branch valleys that are observed in consecutive time slices, wherein the interfluves were incised to form the tributary valleys (Figure 6(A1,B1)). The uppermost and central part of this fluvial channel displayed slimmer channel-belt sizes with plenty of tributary channels, which correspond with a reduction in sinuosity with fewer tributary channels and an increase in the width at the downstream, as shown in Figure 6(A2,B2).

This figure shows that the valley's width can control bar expansion and transition and thus the channel sinuosity. In the southern part of the channel system, a noticeable expansion of the valley can be seen, whereby sinuosity and meander decrease towards the downstream at the south. The eastern segment displays the channel's best image, abandoned channel, bars expansions, and channel belt extended from north to south with a high meandering degree as shown in Figure 6(A3,B3). The slides C1, C2, C3, and C4, are recent analogs with analogous features and similar depositional features: Muar River, Johor, Negeri Sembilan Pahang in Malaysia. A good display in Figure 7 of a 3D block diagram demonstrating the relationship between shape-filled channels in the cross-sections and their chart-view interpretation was noticed at TWT -138 ms. Obviously, the channel's seismic amplitude is quite different from the surrounded point bars' deposits in both the 2D seismic sections and the 3D time slices. The time slice of chart view-imaged Figure 7B represents a well-conserved channel, and channel-belt muddy depositional features, highlighting the channel variation sizes shown in Figure 7B. In the minor channels, there are several of the incised tributary valleys in the single southwest channel: extension surfaces, meander scrolls, abandoned channels, and bar expansions. The 3D amplitude volume reveals the biggest sinuosity channel crosses the Melor field. The blue colors indicate the meander scrolls, while the yellow color infers the sandy bodies filling the channel parts while others are filled with clay. The smaller chart in Figure 7D is an interpreted edition of the 3D seismic amplitude volume, displaying sand-prone facies in orange, mud-prone channel facies in blue, point bars in yellow, and the interfluve in gray and orange.

The carved fluvial channel has a channel belt average width to channel ratio of 1:10 and a depth ratio between channel and valley of 1:2. About 20 m of the point bar thickness comprises 3:1 ratios of the valley fill, while the upper section is characterized by fluvial and marine mudstones (Figure 8A,B). The internal configuration of the reflections, which are characterized by continuous high to moderate amplitude type, showed that these deposits are alternating sediments of the silt and mud, while the main valley has no multi-historic fluvial stack deposits. Three major genetic elements can be differentiated: an early fluvial phase accompanied by a transgressive phase, estuarine deposits overlaid partially on fluvial deposits and formed onlaps on the earlier deposits, and a final open-marine succession that covered the whole valleys (Figure 9). On this fluvial system (-138 ms below sea level), architectural interpretation of the channels, channel belts, and point-bars was carried out (Figure 10A).

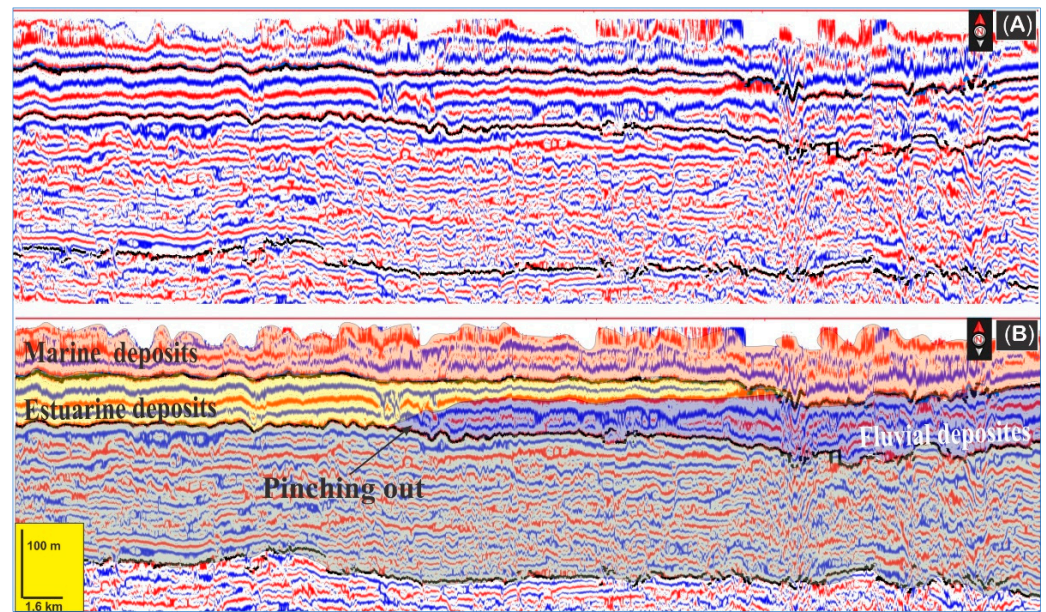


Figure 9. Uninterpreted section in (A), and (B) the interpreted Cosine of Phase seismic attribute cross-section displaying the fluvial depositional system (Blue color). Estuarine deposits formed onlaps against the fluvial channel walls (Yellow). The estuarine and fluvial deposits are laterally capped by marine deposits (Orange).

In the chair display (Figures 8A and 10B), a convex-up geometry represents the incompressible sandy mounded top channel filled with sand. However, the middle did not compress, such as the ends (left and right) of this channel. The concave-up geometry on the right side of the chair display in Figure 10(Bb) represents a compressible muddy-filled channel. In the Inas field direction, time slice with Cosine of Phase attribute inline and cross-seismic sections have been displayed at TWT of -138 ms. In this slice, an apparent meandering channel extended from the southwest to the south exposed over the time slice and cross-section.

Cosine of Phase seismic attributes represent the lateral and vertical dimensions with the incised valley in both inline and Xline. The RGB color attribute shows the time slice at the top and base of the fluvial channel, with the width of this Inas field direction of approximately -50 m. The west-most part of this fluvial channel displayed slimmer channel-belt sizes with corresponding low sinuosity and fewer tributary channels, and an increase in the channel's width and sinuosity at the downstream in the south direction, as shown in Figure 10. The low sinuosity and the narrow width at the west side of this channel are more noticeable at the center and near the downstream, with the morphology at the center and south being flatter. In the southern part of the channel system, a noticeable expansion of the valley can be seen, whereby sinuosity and meander also increase towards the downstream at the south (Figure 10).

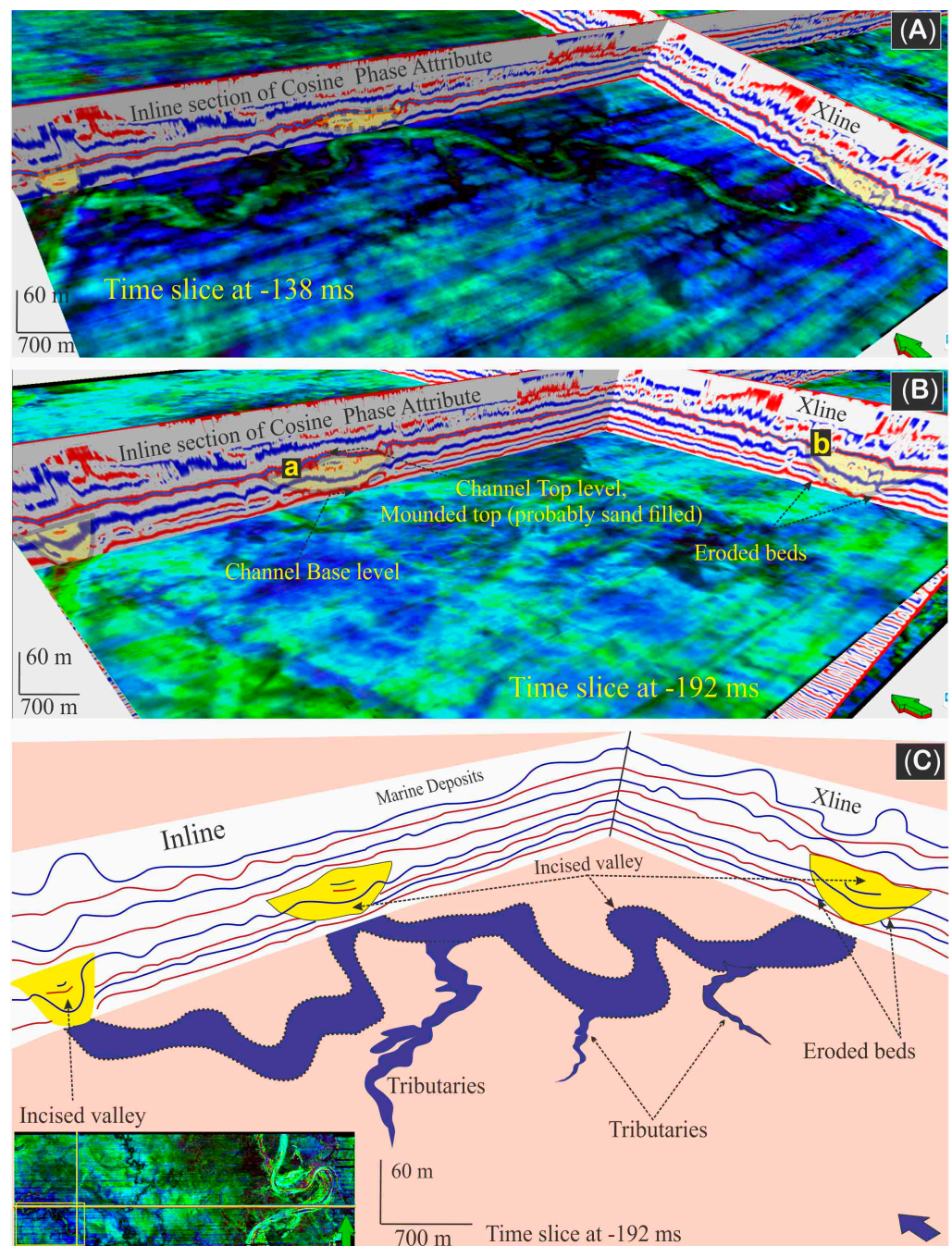


Figure 10. (A) Chair display zoomed-in map-view of the southwest fluvial meandered channel at approximately TWT -138 ms with Xline and Inline Cosine of Phase seismic attribute across the sinuosity channel. The yellow colors represent the repeated channel in both Xline and Inline. (B) Another chair display for lower time slice with the same Xline and Inline Cosine of Phase seismic attribute, channel top-level showing a mounded top (Ba), which is probably filled with sand in the middle and clay in compressed ends. (C) The incised valley with its tributaries in blue color. The eroded beds formed reflector terminations down-laps against the incised valley walls.

4. Seismic Sequence Stratigraphy

4.1. Seismic Facies Classification

Analysis of 2D seismic sections enabled five seismic facies to be distinguished depending on the inner and external geometries with termination patterns from the Melor and Inas fields (Figure 11). These facies include: (1) chaotic seismic facies associated with low-amplitude reflections (these kinds of facies are usually associated with high-energy

deposition environment of point-bar tops) [20]. These facies are acoustically extremely impenetrable and have incoherent internal reflections. (2) Convergence facies with high-amplitude, low-frequency, semi-continuous reflections with single directional onlap against the channel walls. An internal convergence in the upper part of this deposit forms the point bar around the incised channel. (3) Concave-up multi-stacked channel with medium-amplitude and medium-frequency inclined seismic facies. Multi-stacked channel deposits, concave-up geometry with onlaps on the channel walls (usually linked to strike viewpoint crosscut across the middle of point bars). (4) Parallel continuous high-amplitude, low-frequency sheet drape is commonly formed by fine-grained sediment deposited slowly [46]. (5) Laterally continuous seismic facies with medium amplitude and high frequency. These facies are commonly associated with open marine deposits, as shown in Figure 11.

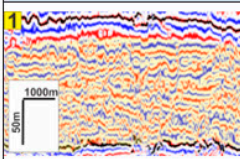
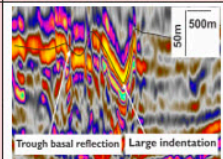
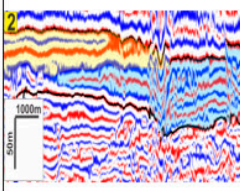
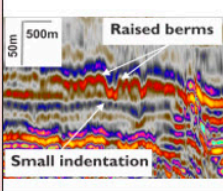
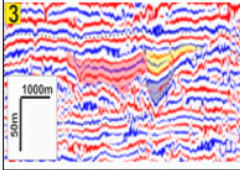
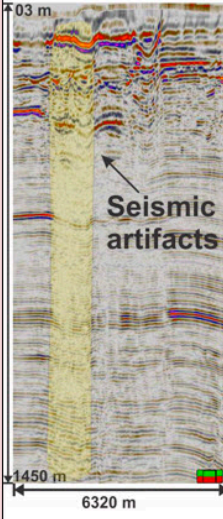
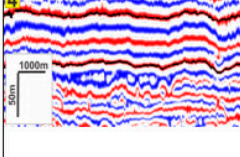
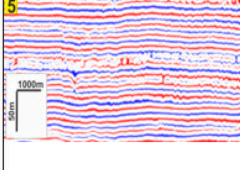
2D- Seismic Facies	Reflection Character/ sedimentologic Interpretation	Seismic Features	Example	Description
	Low- amplitude, medium frequency discontinuous chaotic seismic facies in the yellow color Reworked point bar top deposit.	1)- Large indentation		Large indentation on the trough's basal reflector. Truncate underlying reflections. Widths of up to 700 m, depths of up to 60 m.
	High amplitude, low frequency, semi-continuous with single directional onlap against the channel walls An internal convergence in the upper part. This deposit is forming the point bar around the incised channel.		2)- Small indentation	
	Multi-stacked channel with medium amplitude and medium frequency inclined seismic facies. Concave-up geometry with onlaps on the channel walls	3)- Seismic Artifacts		
	High amplitude parallel Continuous, low-frequency sheet drape which is formed by fine-grained sediment slowly deposited from above.			
	Laterally continuous seismic facies with medium amplitude and high frequency Open marine muddy facies.			

Figure 11. The seismic facies categorization of Cosine of Phase seismic attribute sections depends on continuity, the strength of reflection, and internal reflection patterns. This figure shows five different characterized seismic facies with three observed seismic features.

The seismic facies principles were utilized to analyze and describe the fluvial deposits' internal configurations, such as point bars and multi-stacked channels (Figure 11). Not only that, but it also distinguished the variation between the fluvial, deltaic, and marine seismic reflections. Seismic facies were also essential to explain the different distribution of the depositional environment in space and time within the sequence stratigraphic context.

The concave-up geometry of the multi-stacked channel features a seaward slope increase ranging between 1.23° and 1. –90° at the top of the multi-stacked channel, and from 0.41° to 0.97° towards the bottom. In comparison, on the point bar side, time slices show chaotic configurations with medium amplitude in the upper part of the point bar. The

noticed incline angles extend from 0.35° to 0.50° at the top of the point bar. Nevertheless, since most seismic reflections are not oriented to absolute dips, these slopes' real angles are possibly slightly higher. Furthermore, referring to the previously mentioned geometric variations, scale and areal extent are two of the main variations between the multi-stacked channel and the lateral accretion point bar. Individual sigmoidal geometries extend from the east to south in slide three within Figure 11, forming an onlap against the channel walls.

These reflections are overlaid by convergent reflections below the unconformity and over the fluvial system point bar. This sigmoidal geometry extends horizontally to about 5.3 km from the fluvial channel system. It was truncated by erosion and terminated under the convergent feature as onlaps on the old deposits (Figure 11 slide 2). In contrast, single horizontal accumulation point-bar fluvial surfaces seldom surpass 350 m in depth from up to the base. Besides, the topmost truncated multi-stacked channel in slide 3 characterizes the conserved component of the mouth bar's thicker deposits, which implies that the initial multi-stacked channel sizes were more extensive (Figure 11).

The smallest area assessed on the mouth bar (dependent on several 2D lines of previous studies) is approximately 12 square kilometers. The point bar zone covers only 7.3 square kilometers. The conserved thickness of the multi-stacked channel sediments is 120 m, as shown in Figure 11 slide 3, while point bars are not greater than 49 m. Large indentations truncated underlying reflections with widths of more than 700 m and depths of more than 60 m. Small indentations have maximum widths of 200 m and depth of more than 30 m. Small indentations often have berms a few meters high on either side of a central downturn.

A seismic artifact is shown horizontally along the channel direction and vertically to around 1450 m, and a sample of these artifacts is displayed in slide three of Figure 11 under the seismic features' classification. This artifact is due to seismic processing problems [12], where this pseudo-channel is interpreted as a shadow of the above-observed channel at -138 ms. The internal structure of modern sandy point bars reveals erosional base layers and horizontal surfaces with sudden lateral incline changes. Bridge (1995) [47] interpreted these variations as a distinct event in barrier consolidation and degradation linked to flooding recurrence successions between decades and centuries. 2D and 3D seismic volume, the outcrop descriptions, and borehole evidence have been employed to examine the internal reflection configuration of old marine-impacted point-bar sediments. They describe the horizontal accretion surfaces in inclined convex-up bed sets.

4.2. Sequence Stratigraphy Interpretation

Based on the seismic reflection termination geometries interpreted in 2D sections, seismic facies can be interpreted by integrating 2D with the derived 3D map-view of the depositional system [31,48–52]. Three depositional sequences (DS.1, DS.2, and DS.3) with related system tracts were identified in this examination. Sequence boundaries constrain such sequences (SBs), defined depending on the following principles: (1) The high-frequency reflections (stratigraphic discontinuities) and basal erosional patterns noticed on the 2D seismic section, (2) the presence of map-view trunk fluvial deposits supplied by countless carved branch valleys situated on related interfluves and exhibiting dendritic canyons in time-slice view [7], and (3) the existence of over-consolidated horizons during subaerial display is expected to result in the development of soil evaluated by geotechnical well soil properties [53]. On average, deposition sequence thickness is around 20 m and infrequently comes up to 40 m.

Traditionally, sequences that include a basic sedimentary fill reveal basal valley-bound fluvial layers and are superimposed by estuarine, and subsequently deposit marine and/or periodic concave-up multi-stacked channel deposits. Fluvial deposits of the low stand (convex-up horizontally deposited layers and single or bidirectional down-lap seismic facies) are usually superimposed (SBs) and covered by transgressive surfaces. These deposits are followed by estuarine sediments that are mud-pronounced and correspond to transgressive system tracts (TST) (restricted horizontally continuous seismic facies).

The maximum flooding surface (MFS) covers the fundamental TST and is then overlapped with a high stand system tract of open marine mudstone deposits. The seismic nature of the seismic facies at the top of the high stand shows a rise in contrast in acoustic impedance, possibly reflecting the late phase of the high stand systems tract (HST). However, a detailed explanation of the studied succession, which started from the seafloor to approximately -507 ms, is presented, with three primary seismic stratigraphic sequences and their associated systems tract. From bottom to top, the SB-3 represents the horizon as unconformity separating, unit 3 from unit 2. The surface was identified based on the generated synthetic seismogram of Inas-8, Melor-2, and Melor-1 wells, and the seismic facies' variations of this unit, as shown in Figure 12. This event was interpreted on the largest peak between two intense trough amplitude events representing an interface between unit 3 and unit 2. This unit is extended from the time of -400 to -490 ms.

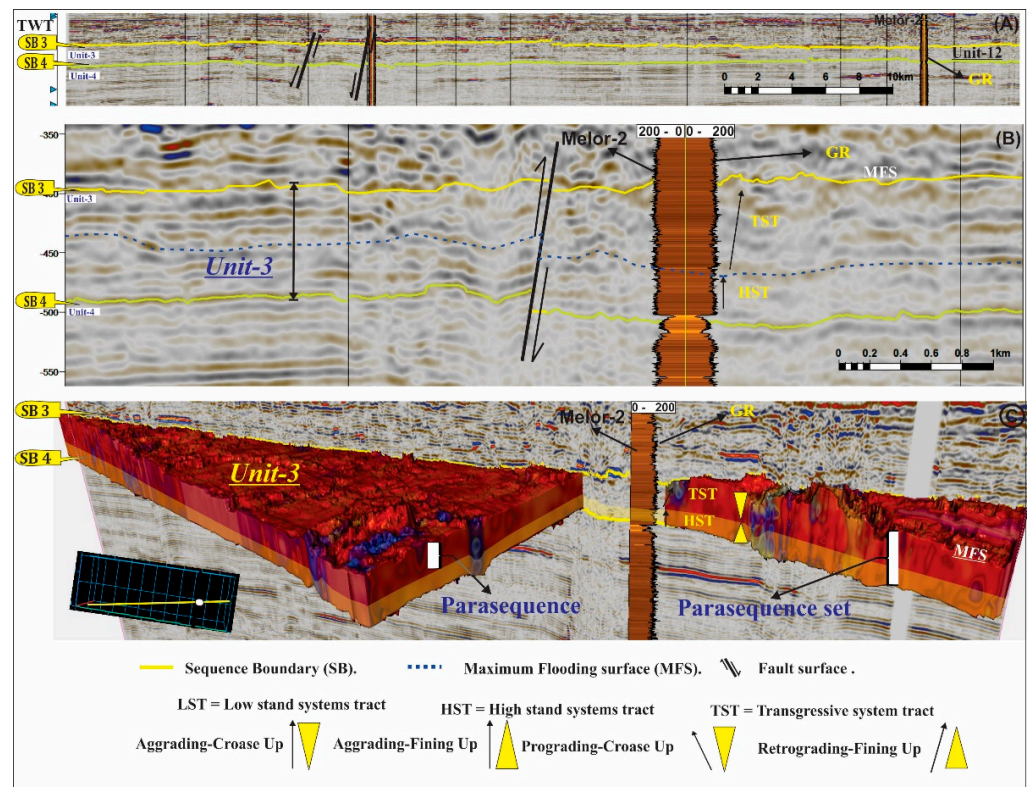


Figure 12. (A) A regional seismic cross-section of unit 3, (B) a detailed explanation of the sequence boundaries of unit 3, systems tract, and faults, and (C) the 3D visualization of unit 3 with system tract, parasequences, and parasequences set.

In terms of the system tract, unit 3 has been divided into only two cycles. This unit's base was formed during the regression phase, while the sea level was prograding seaward, resulting in a High Stand System Tract (HST) cycle. The HST is represented by the coarsening upward of the gamma-ray.

The other cycle in unit 3 is labeled as TST, which forms the top part of this unit. The top of this cycle is marked as a Maximum Flooding surface (MFS) in Figure 12B,C, that caused a retrograding stacking pattern of TST. This cycle yield after the sea level occupied the Malay basin during the connection with the China sea resulted in a TST.

Horizon 2 represents the SB2 surface that bounded at the top of unit 2. This horizon was picked based on the gamma-ray record on Melor-2, the generated synthetic seismogram of Melor-1 well, and the seismic facies' variations of unit 2 (Figure 13).

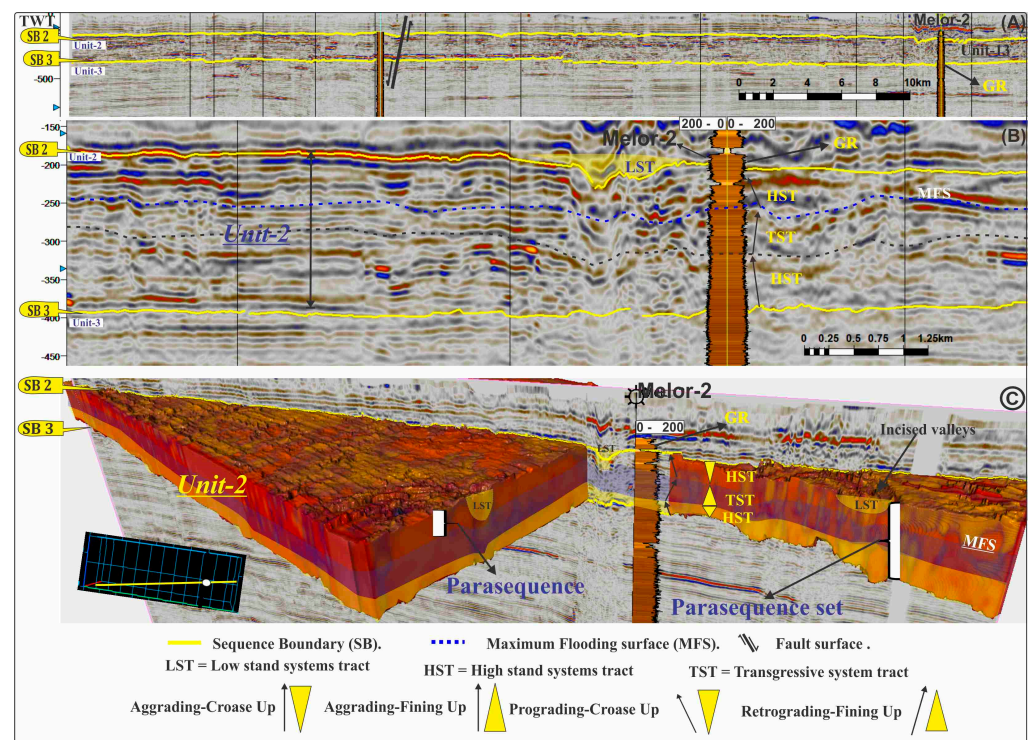


Figure 13. (A) A regional seismic cross-section of unit 2. (B) A detailed explanation of sequence boundaries of unit 2. (C) Visualization of unit 2 with systems tract, faults, parasequences, and parasequences set.

This event was interpreted based on the zero-crossing below a strong trough amplitude event, representing an interface between unit 2 and unit 1. Incised valleys cut the SB-2 and channels, considered as the LST system, as shown in Figure 13B,C. Unit 2 extended from -175 to -400 ms. In terms of the system tract, unit 2 has been sub-divided into three cycles. The base of this unit was formed during the regression phase while the shoreline which was prograding seaward resulted in an HST cycle. The coarsening upward of the gamma-ray record reveals good evidence of this interpretation, which means that this cycle yield after the sea level decreased and continental deposits occupied the Malay basin.

Another cycle of unit 2 was labeled as TST. This cycle formed during a transgression caused by the sea level rising and occupied the Malay basin during the retrogradation session. The TST is characterized by a noticeable fining upward of gamma-ray reading. The top part of this cycle is labeled as MFS and capped this TST cycle. A new coarsening upward in the gamma-ray record reveals another HST in this unit with decreased sea level associated with land sediment deposits. This cycle formed some down-laps reflection terminations seaward against the MFS, reflecting a regular regression session that happened and resulted in prograding stacking patterns of HST, as shown in Figure 13.

This event was interpreted as SB1 on the most significant peak amplitude, representing an interface between unit 1 and the seafloor bed. This horizon represents the sequence boundary bounded at the top of unit 1. SB1 was picked based on the reflector amplitude event, gamma-ray record on Melor-2, the signature of synthetic seismogram of Melor-2 well, truncation reflection termination against the SB1, and the seismic facies' variations (Figure 14). Unit 1 has fantastic features, as displayed in Figures 6–8 and 10. This unit extends from the time of -125.27 to -193.35 ms.

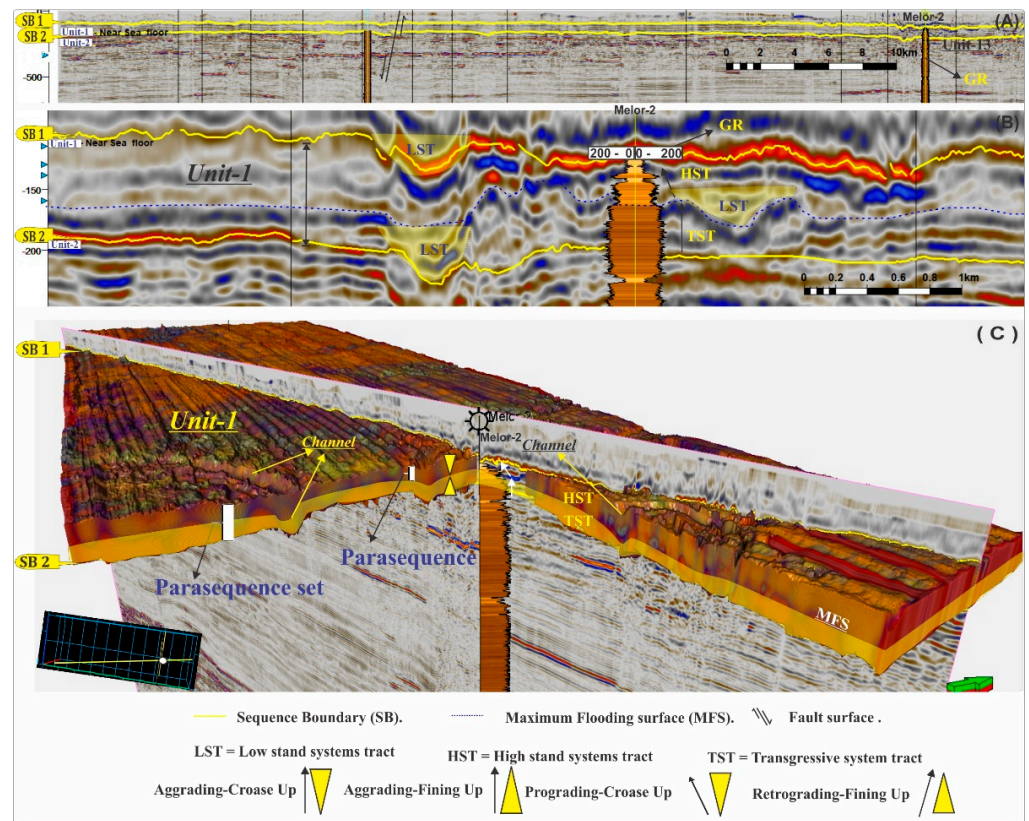


Figure 14. (A) A regional seismic cross-section of unit 1. (B) A detailed explanation of the sequence boundaries of unit 1 and its systems tract. (C) The 3D visualization of unit 1 with systems tract, channel, parasequences, and parasequence set.

Incised valleys cut unit 1 and some other channels, which is interpreted as LST at the top and the bottom of this unit, as shown in Figure 14B,C. This unit was subdivided into two cycles only. The bottom cycle of this unit was labeled as TST associated with a remarkable high gamma-ray record. The bottom of this unit is cut by an incised valley, which is assigned as LST. This cycle was formed during a transgression phase when the sea level was retrograding landward, resulting in a TST cycle. MFS binds this cycle. This cycle is overlain by new HST formed during the new regression phase when the sea level was prograding seaward, resulting in an HST. This cycle is cut by some channels interpreted as LST (Figure 15B,C).

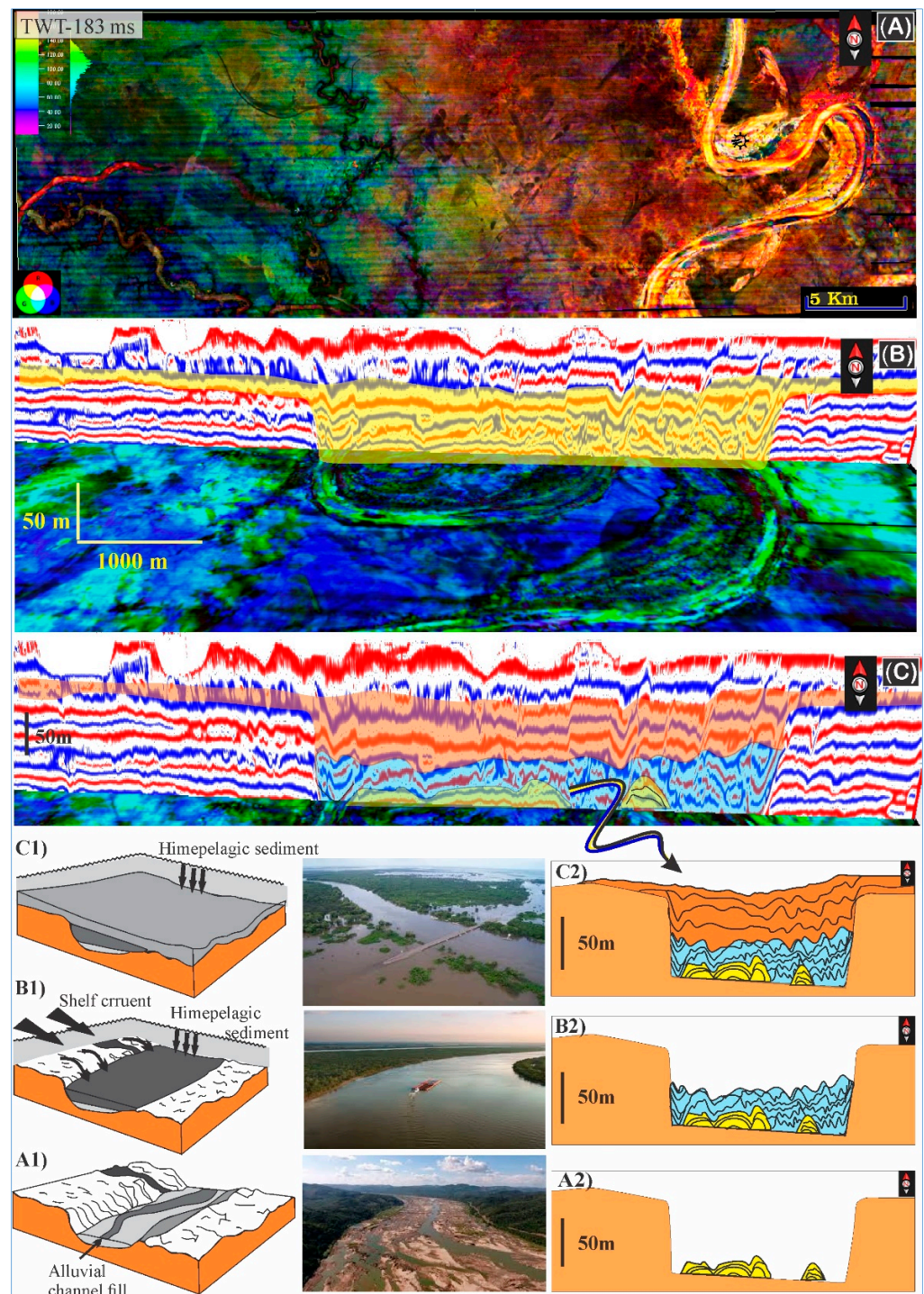


Figure 15. The RGB color blending time slice and Cosine of Phase seismic attribute cross-line through the incised channel, showing the evolution of three separate valley-fill stages: (A) accumulation of point bars throughout active fluvial sediments Lowstand Systems Tract (LST). (B) Transgressive sediments inactively forming reflection of onlaps against the channel walls. (C) Sediments of open-marine high stand covering the whole carved-valley complex. (A1,A2), (B1,B2), and (C1,C2) are simulation diagrams that show the incised valley evolution after [10,16].

5. Discussion

5.1. Incised Valleys Identification

The exceptionally broad incised valleys often reach hundreds of kilometers [54,55]. Some of them are more than 100 m deep [51]. Other identified depths are only ten meters,

such as those in References [24,55,56]. The shallow valley (<35 m) identified as a multi-storied channel deposit in this research shows a simple valley filling with single fluvial deposits on the base. These deposits are superimposed by valley deposits, such as estuarine facies, and covered with open-sea siltstones (Figure 15). The attribute slides in Figure 15 reveal the RGB color time slice with an accumulation of point bars throughout active fluvial sediments interpreted as low stand, as in slide (A). Transgressive sediments inactively form a reflection of onlaps against the channel walls, as shown in slide (B). Slide (C) explains sediments of open-marine high stand covering the whole carved-valley complex. However, simulation diagrams in (A1, A2), (B1, B2), and (C1, C2) are illustrated, showing the incised valley evolution from the bottom (A1, A2) to the top (C1, C2).

This research's standard method to interpret the river systems as a sub-surface carved valley, as seen at -138 ms (Figure 5E,F) and observed within DS.1 (Figure 3B), is listed below.

The incision of the valley is displayed in the 2D seismic cross-section and 3D time slices:

1. The tributary channels' existence passes through the floodplains, as shown in Figure 10, resulting in an abandoned floodplain and functioning as interfluves [7].
2. The interpretation of the abandoned floodplain relies on the sequences regional slope towards the incised channel and channel belt (Figure 9) and the absence of higher topographical levees, in addition to the over-bank presence.
3. The point bar tops that lay at the middle height of the interfluve, as shown in Figures 8 and 15, and paleoenvironmental situation, all revealing that the river could not overtop the precursor floodplain even at the maximum flood phase.
4. The presence of transgressive seismic facies in the valley with draping point bar deposits of the channel and onlapping the walls' valley indicates confinement, possibly associated with an estuary environment.

5.2. 3D Data Horizontal Time Slices Evidence (Map-View)

1. Existence of little carved tributary valleys stretching up to 2.5 km from the main body valley (Figure 5H, Figure 6, Figure 7, and Figure 10). The erosional characteristics indicate that the flood plains had been absent and categorized by constant drainage systems.
2. The presence of sinuosity and meandering of channel shapes are implying the incised valleys were passing and cutting sheet-like geomorphological floodplain deposits (Figures 6–8 and 10). The areas with less sinuosity infer a higher slope than in the high meandered segments.

The degradation implied nature and an essential feature of these fluvial systems and the whole sequences. The channels and channel belts are perpendicularly constrained in the lower places within every sequence and are methodically situated in valleys, without any proof of the fluvial floodplain deposits' aggradation outside these accommodations. The distinguishable pattern of degradation stacking in Figure 3B reveals that TST and LST are conserved just within the valleys. Simultaneously, the whole aggradation is severely restricted to the HST sea mudstones.

5.3. Accommodation and Conservation Possibilities

Some significant factors influence and control the creation of extensive succession sequence stratigraphic discontinuity and incised valleys within the tectonic shelf. These include eustasy, subsidence, climate changes, supply, and sediment discharge. In most cases, the fluvial discharge is associated with climate changes, and both influence and dominate the fluvial incision depth, the dimension of the valley, and the number of depositional elements. Subsidence controls the whole succession thickness, while the eustasy regulates the frequency of the stratigraphic event that interrupts the succession.

These factors combined regulate the entire accommodation on the shelf and regulated the conservation capability of distinct depositional environments and systems tracts. Conversely, eustasy's task quickly decreases up-river as locality influences such as climate and tectonics control have more impact [38,57].

Recent researchers concentrated on Southeast Asia and highlighted the significance of some controlling factors such as fluvial discharge and climatic changes on the incised valleys' formation, rather than eustatic sea-level drops [56,58,59]. Interpretation indicates that valleys and incisions appear throughout peak fluvial discharge times, irrespective of the location of the sea level [60].

The melted ice in the glaciated territories is the key control for the discharge alteration, while the climate changes can have the same effect in non-glaciated territories [56].

Climate change may happen at any time throughout a sea-level process and is not directly connected to glaciation or deglaciation cycles. However, it is proposed that substantial climate changes occur during the Pleistocene transformation to Holocene, more probably than during a particular low- or high-stand era of sea levels. In the history of fluvial valley incision, it is difficult to list the different impacts of sea-level change and climate change. In 1999, Posamentier and Allen [57] proposed that sea level alterations are the major cause of river incision in down-stream segments, while climate change and tectonics contribute significantly to upstream sections.

The incision's relative depths in the shallow parts of the channels seen here are about <45 m. This can be interpreted by the absence of a nearby knick-point in the low slope ($\sim 0.006^\circ$) of the Malay Basin.

Due to this low basin gradient, the coastline can move huge distances with just slight relative sea-level changes, revealing or flooding huge regions in short times [61–63]. Besides, the relatively little distance occupied by carved draining valleys may indicate short-lived sea levels compared to the area of main river systems. Indeed, the relatively little distance occupied by carved tributary valleys equated to the area of river trunk systems assumes shorter sea levels of the low stand.

Conversely, the restricted magnitude of incised tributary valleys suggests that the reasons for fluvial incision were short-lived climatic changes and their role in fluvial discharge differences rather than eustasy. This does not mean that the eustasy does not influence at all. The function of sea-level change resulted in a tremendous shift in the coastline over time. Therefore, coastline deposits seemed to increase either thousands of kilometers downstream of this studied area (throughout sea-level low stands) or near the most resonant side of the shelf, around hundreds of kilometers upstream from the studied area (during a high stand of the sea level of the shelf). After intricately carved valleys have been formed, they are initiated to fill strictly by estuarine and fluvial deposits [64].

The apparent imaging of the fluvial depositional features contained by incised valleys such as in Figure 5A–H proposed a high conservation possibility of fluvial sediments but restricted just to carved "containers" [7]. On the other hand, the non-existence of distributive channel structures or delta lobes between high stand sediments and the subsequent LST fluvial sediments indicates a slight preservation possibility in this region of regressive deltaic sequences.

From the inner to mid-shelf, which symbolizes the study region, the coastline was possibly not motionless, but in a quick move, either transits seaward throughout sea-level drop or towards the land side throughout sea-level increase. This is particularly common in the lower slope shelf conditions, as discussed previously, in which even small changes in sea level led to massive shifting in the coastline. Even so, it could not be eliminated that perhaps the coastline might have stopped in this region. However, there is no substantial history of this time that has been kept for such a short time. It can, therefore, be mentioned that the stratigraphic portion of this study area is characterized by the landward sections of the LSTs, such as incised fluvial valley filling, and by the seaward parts of the HSTs. In this region of the Malay Basin, stratigraphic construction (Figure 3B) is described as aggregation ultimately constrained to marine sedimentation at a high stand of sea level.

Throughout LST, the fluvial systems usually tend to behave, such as a circumvent system with minimal deposition, transporting sediment through shallow incised valleys to the paleo-shoreline. Preserved fluvial sediments typically correlate to late phases of LST of the sea levels when the accommodation creation rate rises. SBs stretch laterally through

interfluves from the bottom of the incised valleys and then integrate with the transgressive cycle's surfaces. The TST is only depicted in this part as estuarine covers of carved valleys with minimal or no accumulation of equivalent interfluves (Figure 9).

The surfaces of the sequence-stratigraphic units, such as sequence boundaries, incised valleys, and overall flooding surfaces, are determined by the scale and resolution of the used data. Chen et al. classified the succession into three sequences, two only within the TWT of the first 500 ms from the seafloor, equal to an average of around 4.9 M.Y./Sequence [65]. However, this research showed that higher resolution sequences are presented within the 2D seismic sections. The 2D high-resolution sections with cosine phase seismic attribute allowed us to subdivide the interested succession (Group A) into three major sequences. These units were composed (3rd order) with four parasequences sets (4th order) and seven parasequences (5th order), as shown in Figures 3 and 12–14. Magnitudes of LST deposits of sea level were big enough to expose in the current succession at around −90 ms to −241 ms in the sub-buried shelf in the study area. Therefore, the period interpretation describing the studied segment.

As a consequence, many other smaller sequence scales (20–40 m thick), such as parasequences and parasequence set, of the marine regression and transgression within all sequences have been illustrated by Chen et al. and can probably be associated with the low lodging, low slope, and also low subsidence ratios [65].

5.4. Exploration Effects of Hydrocarbon

Understanding the mechanics of the fluvial system helps predict the distribution of both the sandstone and the reservoir. The detailed 3D interpretation and identification of subsurface sandstone bodies help us make sense of reservoir interconnection. The deposited beds' encountered discontinuities may have resulted due to the mud-drape deposition throughout the weak condition of flow hydrodynamics [39]. This may affect the reservoir's connectivity. Like abandoned channels of mud plugs and engraved valley walls, the wide discontinuities may function as horizontal stratigraphic caps for the sandy channel belt bar sediments. This case eventually leads to a characterization of the reservoir system.

In the exploration and field development of hydrocarbons, it is a common pitfall to presume that channels that are imaged in 3D seismic time slices are uniform reservoir-filled components. There is a tendency to ignore the intrinsic complexity of channel storage tanks. The observations introduced here outline that this complexity can be very useful in establishing a more accurate and consistent static model of reservoirs. By integrating the high-resolution 2D seismic sections and 3D time slices of this study, concluding that point bar sediments represent reservoir-prone elements, the channels seem to be filled with mud deposits similar to the filling process of the abandoned channels.

The mudstone-filled channels repeatedly cut through the point bars' sand bodies and probably separate the points bars from each other, segregating reservoir bodies. The mud plugs act as walls or barriers to some extent based on the natural surroundings' sediments. Channel lag sediments can typically work as linkages between the point bar's storage containers at the abandoned channel's base [66]. While these lags of channels are continuously totally linked and consistent, these plugs of the abandoned channels can function as barriers to the hydrocarbons' flow, where lags are discontinuous to nonexistent.

This study also suggests that some successions show no complete system tract. HST deposits are characterized primarily by proximal marine non-reservoir elements, while the fluvial incised valley-filling deposits represent LST deposits. The transgressive systems tract (TST) deposits seem confined to incised valley non-reservoir sediments, which are usually found superimposed on the fluvial low stand deposits.

6. Conclusions

This investigation incorporated geomorphological images of the depositional systems from the 3D seismic volume (time slices) with detailed seismic facies classification of the fluvial point bar sediments. The sequence stratigraphy of 3rd, 4th, and 5th orders

with systems tract detail analysis from the high-resolution 2D seismic sections has been conducted as well. The approach allowed us to accurately interpret such lateral and vertical heterogeneous deposits with different geomorphological elements that were observed within time slices and 2D seismic sections.

A chronological framework was established by describing high-resolution sequence stratigraphic discontinuities using high-resolution 2D seismic sections for roughly –507 ms (522 m) thick succession. The utilized approach led to an accurate correlation of the geomorphological features encountered on time slices with certain sequence surfaces in the seismic sections. Furthermore, the identification in the surfaces' section views explained the spatial relation between channel belts and channels detected in the same 3D time slices.

Therefore, we can conclude that these channel belts exist in several sequences and are not simply mounds of auto-cyclic rapid abandonment of a fluvial channel system.

The predominant sediment types in these fields are high stand of the distal shelf, shallow marine deltaic deposits, and fluvial low stand incised valley deposits. Small quantities of estuarine sediment were found overlying the incised valleys. The production of new sheet accommodation generally takes place throughout the transgressions and subsequent high stand phase, where minimum accommodation is confined to mostly incised valleys in the low stand phase.

The geomorphological elements observed are comprised of fluvial point bars, tide-influenced point bars, plugs of the abandonment mud, mouth bar clinofolds, estuarine valley fills, channels, and channel belts. The reflection terminations' geometry can distinguish the reflection configuration of the distinct clinofold and point bars. Thus, convex-up geometries characterize the point bars, while concave-up geometries distinguish the clinofold mouth bars. Besides, point-bar horizontal accumulation surfaces are likely to have preserved the down-laps, whereas the mouth bar's clinofold seems to exhibit a long extension of reflection terminations of top laps and onlaps.

Incised valleys in this section of the basin are common features. A comprehensive channel belt analysis observed at –96 ms shows that the channel belt is a single-story system situated in a shallow valley (Figure 5). The features used to identify the incised valleys included the existence of carved-out branched tributary valleys, non-existent levees, and related over-bank sediments.

The occurrence of the point bar top deposits at the middle of the interfluvial level, the valley fills presence, which contains the fluvial phase, and estuarine deposits with a regional tendency of interfluvial to the incised valley direction. The increase of fluvial discharge associated with climate changes was perhaps the most probable influence for valley formation. Such differences are overlaid on the accretion of sequences consisting of continental cycles to marine successions related to changes in high amplitude and high frequencies of the sea level.

Two primary control factors include the amount of erosion along the boundaries of the sequence and the different accommodation styles developed at different times. These impact the degree of systems tract (TSTs, LSTs, and HSTs) for all depositional sequences. Despite the apparent evidence of the fluvial and distal marine deposition, marine sediments' nearshore evidence was not observed. That may be related to the rapid shoreline movement recorded over the study area, which rarely existed long enough to allow for significant deposits. Similarly, even though accommodation development throughout periods of transgression was generally restricted to flooded valleys, transgressive systems tract TST sedimentations are only slightly observed here, capping the incised valleys' tops.

The predominant fluvial type in this region is single-channel fluvial systems associated with flanks and point bars. Together with this sedimentary system style, abandoned channels are pervasive. Understanding that the abandoned channels are generally filled with mud has significant outcomes for exploring and developing hydrocarbons to locate the sand bodies as hosts for the oil and gas. The injected muds within the channels can function as permeability or fluid flow barriers to the hydrocarbons' migration.

Based on the obtained results that utilized the proposed approaches, we firmly believe that proposed approaches can be implemented practically in other field investigations due to the high accuracy and reliability achieved in this research. However, some limitations restrict the adopted approaches from reaching the optimal level and some suggestions that we believe will serve for future work were presented.

This research mainly emphasizes reducing the studied area's uncertainty and ambiguity by establishing reliable seismic sequence stratigraphy and depositional environment geometries frameworks. Besides the studied area's complexed nature, there is a shortage of detailed investigations clarifying understanding the potential hydrocarbons reservoir distribution in interbedded sand and clay deposits. Although the proposed approaches can perform a reliable interpretation and reduce uncertainty, we still believe that they can be further improved by incorporating as much as we can of the required data and implementing the machine learning techniques to achieve more interpretation accuracy in a short time and with less effort.

Author Contributions: Conceptualization, A.A.-S.A.-M., M.E., A.A.B., and S.E.; methodology, A.A.-S.A.-M.; software, A.A.-S.A.-M., A.A.B., I.B., and Q.S.I.; validation, A.A.-S.A.-M., A.A.B., N.A.S., and T.A.; formal analysis, A.A.-S.A.-M. and S.E.; investigation, A.A.-S.A.-M.; resources, A.H.A.L.; data curation, A.H.A.L.; writing—original draft preparation, A.A.-S.A.-M.; writing—review and editing, A.A.-S.A.-M., M.E., N.A.S., and S.E.; visualization, A.A.-S.A.-M., I.B., and A.A.B.; supervision, M.E., N.A.S., and A.A.B.; project administration, A.H.A.L.; funding acquisition, A.H.A.L. and M.H. All authors have read and agreed to the published version of the manuscript.

Funding: This research was supported through the following projects: Centre of Seismic Imaging with cost center (0153C1-027), Artificial intelligence on seismic attributes with cost center (015MD0-057), (YUTP Cost #015LC0-220), Incorporating Anisotropy Effect in AVO Analysis for Hydrocarbon Prediction with cost center (015LCO-224), Petroleum Research Fund (PRF) (Grant No.0153AB-A33) awarded to Associate Professor Eswaran Padmanabhan and the Fundamental Research Grant Scheme (FRGS), Ministry of Higher Education (MoHE), Malaysia (Project ID 16880, Reference Code FRGS/1/2019/STG09/UTP/03/1).

Institutional Review Board Statement: Not applicable.

Informed Consent Statement: Not applicable.

Data Availability Statement: The associated data in this study are confidential and cannot be released.

Acknowledgments: The authors are so grateful to Universiti Teknologi Petronas and the Centre for Subsurface Imaging (CSI), Malaysia, for providing the required data for this research. We would like to express our admiration to the Geoscience Department, Universiti Teknologi PETRONAS colleagues for supporting us during this research with cost centers (0153C1-027), (015MD0-057), and (015LCO-224). The authors would like to thank Petroleum Research Fund (PRF) (Grant No.0153AB-A33) awarded to Associate Professor Eswaran Padmanabhan and the Fundamental Research Grant Scheme (FRGS), Ministry Higher Education (MoHE), Malaysia (Project ID 16880, Reference Code FRGS/1/2019/STG09/UTP/03/1); for financial support. The authors declare no conflict of interest and, thanks to anonymous reviewers, are thanked for their comments. We acknowledge Schlumberger and Eliis Companies for providing Petrel and PaleoScan™ software licenses.

Conflicts of Interest: The authors declare no conflict of interest.

References

1. Alqahtani, F.A.; Johnson, H.D.; Jackson, C.A.; Som, M.R.B. Nature, origin and evolution of a Late Pleistocene incised valley-fill, Sunda Shelf, Southeast Asia. *Sedimentology* **2015**, *62*, 1198–1232. [[CrossRef](#)]
2. Babikir, I.A.M.; Salim, A.M.A.; Ghosh, D.P. Lithogeomorphological facies analysis of Upper Miocene coal-prone fluviodeltaic reservoirs, Northern Malay Basin. *Interpretation* **2019**, *7*, T565–T579. [[CrossRef](#)]
3. Wu, X. 3D seismic image processing for interpretation and subsurface modeling. In *SEG Technical Program Expanded Abstracts 2017*; Society of Exploration Geophysicists: Tulsa, OK, USA, 2017; pp. 1865–1871.
4. Zeng, H. Seismic imaging for seismic geomorphology beyond the seabed: Potentials and challenges. *Geol. Soc. Spec. Publ.* **2007**, *277*, 15–28. [[CrossRef](#)]

5. Zeng, H.; Ambrose, W.A.; Villalta, E. Seismic sedimentology and regional depositional systems in Miocene Norte, Lake Maracaibo, Venezuela. *Lead. Edge* **2001**, *20*, 1260–1269. [[CrossRef](#)]
6. Carter, D.C. 3-D seismic geomorphology: Insights into fluvial reservoir deposition and performance, Widuri field, Java Sea. *Am. Assoc. Pet. Geol. Bull.* **2003**, *87*, 909–934. [[CrossRef](#)]
7. Koson, S.; Chenrai, P.; Choowong, M. Seismic Attributes and Their Applications in Seismic Geomorphology. *Bull. Earth Sci. Thail.* **2014**, *6*, 1–9.
8. Liu, S.; Jiang, Z.; He, Y.; Dou, L.; Yang, Y.; Li, Y.; Han, C. Geomorphology, lithofacies and sedimentary environment of lacustrine carbonates in the Eocene Dongying Depression, Bohai Bay Basin, China. *Mar. Pet. Geol.* **2020**, *113*, 18. [[CrossRef](#)]
9. Miall, A.D. Architecture and sequence stratigraphy of Pleistocene fluvial systems in the Malay Basin, based on seismic time-slice analysis. *Am. Assoc. Pet. Geol.* **2001**, *10*, 1771–1793.
10. Posamentier, H.W. Lowstand alluvial bypass systems: Incised vs. unincised. *Am. Assoc. Pet. Geol.* **2001**, *10*, 1771–1793.
11. Posamentier, H.W.; Kolla, V. Seismic Geomorphology and Stratigraphy of Depositional Elements in Deep-Water Settings. *J. Sediment. Res.* **2003**, *73*, 367–388. [[CrossRef](#)]
12. Davies, R.J.; Posamentier, H.W.; Wood, L.J.; Cartwright, J.A. *Seismic Geomorphology: Applications to Hydrocarbon Exploration and Production*; Geological Society: London, UK, 2007.
13. Simmons, M.D.; Sharland, P.R.; Casey, D.M.; Davies, R.B.; Sutcliffe, O.E. Arabian plate sequence stratigraphy: Potential implications for global chronostratigraphy. *GeoArabia* **2007**, *12*, 101–130.
14. Siddiqui, N.A.; Ramkumar, M.; Rahman, A.H.A.; Mathew, M.J.; Santosh, M.; Sum, C.W.; Menier, D. High resolution facies architecture and digital outcrop modeling of the Sandakan formation sandstone reservoir, Borneo: Implications for reservoir characterization and flow simulation. *Geosci. Front.* **2019**, *10*, 957–971. [[CrossRef](#)]
15. Almasgari, A.A.; Elsaadany, M.; Latiff, A.H.A. Application of seismic attributes to delineate the geological features of the Malay Basin. *Bull. Geol. Soc. Malays.* **2020**, *69*, 97–110. [[CrossRef](#)]
16. Reijnenstein, H.M.; Posamentier, H.W.; Bhattacharya, J.P. Seismic geomorphology and high-resolution seismic stratigraphy of inner-shelf fluvial, estuarine, deltaic, and marine sequences, Gulf of Thailand. *Am. Assoc. Pet. Geol. Bull.* **2011**, *95*, 1959–1990.
17. Madon, M.B.H.; Peter Abolins, M.J.B.H.; Ahmad, M.B. *The Petroleum Geology and Resources of Malaysia*, 1st ed.; Petronas Carigali Son Bho: Kuala Lumpur, Malaysia, 1999.
18. Imran, Q.S.; Siddiqui, N.A.; Latif, A.H.A.; Bashir, Y.; Ali, A.A.A.S.; Jamil, M. Integrated Well Data and 3D Seismic Inversion Study for Reservoir Delineation and Description. *Bull. Geol. Soc. Malays.* **2020**, *70*, 209–220. [[CrossRef](#)]
19. Ibrahim, N.A.; Madon, M. Depositional environments, diagenesis, and porosity of reservoir sandstones in the Malong Field, offshore West Malaysia. *Bull. Geol. Soc. Malays.* **1990**, *27*, 27–55. [[CrossRef](#)]
20. Ince, D.; Madon, M.; Rahman, A.H.; Koraini, A.M.; Mohamed, M.; Hassan, S.S.; Wan Abdullah, H.; Jirin, S.; Farah, U. The Possible Significances of Coals Encountered in Cored Sections from the Central Malay Basin; Implications for Sequence Stratigraphic Interpretation and Basin Character. In Proceedings of the Petroleum Geoscience Conference & Exhibition, Kuala Lumpur, Malaysia, 7–8 March 2011; Volume 50526, pp. 151–152.
21. Nair, N.; Pandey, D.K.; Pandey, A.; Prerna, R. Seismic stratigraphy and the sedimentation history in the Laxmi Basin of the eastern Arabian Sea: Constraints from IODP Expedition 355. *Geosci. Front.* **2021**, *12*, 101111. [[CrossRef](#)]
22. Madon, M.; Council, N.S. A review of stratigraphic simulation techniques and their applications in sequence stratigraphy and basin analysis. *Bull. Geol. Soc. Malays.* **2008**, *54*, 81–89.
23. Hutchison, C.S. *Geological Evolution of South-East Asia*; Geological Society of Malaysia: Kuala Lumpur, Malaysia, 2007; Volume 8.
24. Almasgari, A.A.; Mohamed, E.; Latiff, A.H.A.; Siddiqui, N.; Purnomo, E.W.; Alwali, B.I.; Teslim, A.; Qazi, I. Reducing Thin Bed Reservoir Interpretation Uncertainty Using Comprehensive AVO Classification. *Pet. Coal Artic.* **2020**, *62*, 1577–1585.
25. Babikir, I.; Salim, A.; Hermana, M.; Latiff, A.H.A.; Almasgari, A. Multiattribute analysis of a Pleistocene fluvial system using RGB color blending and self-organizing maps. In Proceedings of the SEG International Exposition and 90th Annual Meeting, online. 11–16 October 2020; pp. 1279–1283.
26. Catuneanu, O.; Abreu, V.; Bhattacharya, J.P.; Blum, M.D.; Dalrymple, R.W.; Eriksson, P.G.; Fielding, C.R.; Fisher, W.L.; Galloway, W.E.; Gibling, M.R.; et al. Towards the standardization of sequence stratigraphy. *Earth Sci. Rev.* **2009**, *92*, 1–33. [[CrossRef](#)]
27. Posamentier, H.W.; Allen, G.P. *Siliciclastic Sequence Stratigraphy: Concepts and Applications: SEPM Concepts in Sedimentology and Paleontology*; Society for Sedimentary Geology: Tulsa, OK, USA, 1999; Volume 7.
28. Paul, J.D. High-resolution geological maps of central London, UK: Comparisons with the London Underground. *Geosci. Front.* **2016**, *7*, 273–286. [[CrossRef](#)]
29. Oldknow, C.; Oldfield, F.; Carr, A.; Hooke, J.; Biggin, A.; Boyle, J.; Hunt, A.; Shen, Z. Palustrine wetland formation during the MIS 3 interstadial: Implications for preserved alluvial records in the South African Karoo. *Sediment. Geol.* **2020**, *405*, 105698. [[CrossRef](#)]
30. Posamentier, H.W.; Jervey, M.T.; Vail, P.R. Eustatic Controls on Clastic Deposition I—Conceptual Framework. In *Sea-Level Changes: An Integrated Approach*; SEPM Society for Sedimentary Geology: Tulsa, OK, USA, 1988; pp. 109–124.
31. Steinshouer, D.W.; Qiang, J.; McCabe, P.J.; Ryder, R.T. *Maps Showing Geology, Oil and Gas Fields, and Geologic Provinces of the Asia Pacific Region*; U.S. Geological Survey: Reston, VA, USA, 1997.
32. Loucks, R.G.; Sarg, J.F. *Carbonate Sequence Stratigraphy: Recent Developments and Applications*; No. 57; American Association of Petroleum Geologists: Tulsa, OK, USA, 1993.
33. Neal, J.; Risch, D.; Vail, P. Sequence stratigraphy—A global theory for local success. *Oilf. Rev.* **1993**, *46*, 51–62.

34. Loucks, R.G.; Frederick, J. *Carbonate Sequence Stratigraphy: Recent Developments and Applications*; American Association of Petroleum Geologists: Tulsa, OK, USA, 1994; Volume 57.
35. Aitken, J.F.; Howell, J.A. High resolution sequence stratigraphy: Innovations, applications and future prospects. *Geol. Soc. Lond. Spec. Publ.* **1996**, *104*, 1–9. [[CrossRef](#)]
36. Hesselbo, S.P.; Parkinson, D.N. *Sequence Stratigraphy in British Geology*; Geological Society: London, UK, 1996; Volume 103.
37. Catuneanu, O. *Principles of Sequence Stratigraphy*, 1st ed.; Elsevier: Edmonton, AB, Canada, 2006.
38. Zhao, W.; Zou, C.; Chi, Y.; Zeng, H. Sequence stratigraphy, seismic sedimentology, and lithostratigraphic plays: Upper Cretaceous, Sifangtuozi area, southwest Songliao Basin, China. *Am. Assoc. Pet. Geol. Bull.* **2011**, *95*, 241–265. [[CrossRef](#)]
39. Kabanov, P. Stratigraphic Unconformities: Review of the Concept and Examples from the Middle-Upper Paleozoic. In *Seismic and Sequence Stratigraphy and Integrated Stratigraphy—New Insights and Contributions*; IntechOpen: London, UK, 2017; p. 28.
40. Willis, B.J.; Tang, H. Three-Dimensional Connectivity of Point-Bar Deposits. *Jpn. J. Sediment. Res.* **2010**, *80*, 440–454. [[CrossRef](#)]
41. Shanley, K.W.; McCabe, P.J. Perspectives on the sequence stratigraphy of continental strata. *Am. Assoc. Pet. Geol. Bull.* **1994**, *78*, 544–568.
42. Liu, M.; Li, W.; Jarvis, M.; Nivlet, P. 3D seismic facies classification using convolutional neural network and semi-supervised generative adversarial network. *SEG Int. Expo. Annu. Meet.* **2020**, *2019*, 4995–4999.
43. Posamentier, H.W.; Davies, R.J.; Cartwright, J.A.; Wood, L. Seismic geomorphology—An overview. *Geol. Soc. Lond. Spec. Publ.* **2007**, *277*, 1–14. [[CrossRef](#)]
44. Sam-Marcus, J.; Enaworu, E.; Rotimi, O.J.; Seteyeobot, I. A proposed solution to the determination of water saturation: Using a modelled equation. *J. Pet. Explor. Prod. Technol.* **2018**, *8*, 1009–1015. [[CrossRef](#)]
45. Orsi, T.H.; Dunn, D.A. Correlations between sound velocity and related properties of glacio-marine sediments: Barents Sea. *Geo-Marine Lett.* **1991**, *11*, 79–83. [[CrossRef](#)]
46. Brown, A.R. Tuning Phenomena in Reservoirs. In *Interpretation of Three-Dimensional Seismic Data—Chapter 6*; Society of Exploration Geophysicists and the American Association of Petroleum Geologists: Tulsa, OK, USA, 2011; pp. 199–212.
47. Al-Masgari, A.A.S.; Elsaadany, M.; Abdul Latiff, A.H.; Hermama, M.; Hamzah, U.B.; Babikir, I.; Adeleke, T.; Sohail Imran, Q.; Al-Bared, M.A.M. Seismic sequence stratigraphic sub-division using well logs and seismic data of Taranaki Basin, New Zealand. *Appl. Sci.* **2021**, *11*, 1226. [[CrossRef](#)]
48. Almasgari, A.A.A.S.; Hamzah, U. Sequence stratigraphy of the pliocene deposits, Central Taranaki Basin, New Zealand. *AIP Conf. Proc.* **2016**, *1784*, 060001.
49. Bridge, J.S.; Alexander, J.; Collier, R.E.L.; Gawthorpe, R.L.; Jarvis, J. Ground-penetrating radar and coring used to study the large-scale structure of point-bar deposits in three dimensions. *Sedimentology* **1995**, *42*, 839–852. [[CrossRef](#)]
50. Corbeanu, R.M.; Wizevich, M.C.; Bhattacharya, J.P.; Zeng, X.; McMechan, G.A. Three-dimensional architecture of ancient lower delta-plain point bars using ground-penetrating radar, Cretaceous Ferron Sandstone, Utah. *AAPG Stud. Geol.* **2004**, *50*, 427–449.
51. Morrison, K.; Lee, W.C. Sequence stratigraphic framework of Northwest Borneo. *Bull. Geol. Soc. Malays.* **2003**, *47*, 127–138. [[CrossRef](#)]
52. Blum, M.D. Genesis and architecture of incised valley fill sequences: A late Quaternary example from the Colorado River, Gulf Coastal Plain of Texas. *Am. Assoc. Pet. Geol. Bull.* **1993**, 259–283.
53. Blum, M.D.; Price, D.M. Glacio-Eustatic and Climatic Controls on Quaternary Alluvial Plain Deposition, Texas Coastal Plain. *Am. Assoc. Pet. Geol. Bull.* **1994**, *44*, 85–92.
54. Mitchum, R.M.; Vail, P.R.; Thompson, S. Seismic stratigraphy and global changes of sea level, part 2: The depositional sequence as a basic unit for stratigraphic analysis: Section 2. Application of seismic reflection configuration to stratigraphic interpretation. In *M 26: Seismic Stratigraphy—Applications to Hydrocarbon Exploration*; The AAPG Publications: Tulsa, OK, USA, 1977; Volume 26, pp. 53–62.
55. Vail, P.R.; Mitchum, R.M.; Thompson, S.I. Seismic stratigraphy and global changes of sea level, Part 4: Global Cycles of Relative Changes of Sea Level. In *M 26: Seismic Stratigraphy Applications to Hydrocarbon Exploration*; The AAPG Publications: Tulsa, OK, USA, 1977; pp. 83–97.
56. Van Wagoner, J.C.; Posamentier, H.W.; Mitchum, R.M.J.; Vail, P.R.; Sarg, J.F.; Loutit, T.S.; Hardenbol, J. An Overview of the Fundamentals of Sequence Stratigraphy and Key Definitions. *Soc. Econ. Paleontol. Mineral.* **1988**, *42*, 39–45.
57. Posamentier, H.W.; Vail, P.R. Eustatic Controls on Clastic Deposition II—Sequence and Systems Tract Models. *Soc. Econ. Paleontol. Mineral.* **1988**, *42*, 125–154.
58. van Wagoner, J.C.; Mitchum, R.M.; Campion, K.M.; Rahmanian, V.D. *Siliciclastic Sequence Stratigraphy in Well Logs, Cores, and Outcrops*; American Association of Petroleum Geologists: Tulsa, OK, USA, 1990; Volume 174, p. 55.
59. Zeng, H. Stratal slice: The next generation. *Lead. Edge* **2013**, *32*, 140–144. [[CrossRef](#)]
60. Latiff, A.H.A.; Ghosh, D.P. A Hybrid Approach for Subsurface Illumination Analysis in Shallow Gas Region: A Case Study in Malay Basin. In *ICIPEG 2014*; Springer: Singapore, 2015; pp. 249–256.
61. Anderson, J.B.; Abdulah, K.; Sarzalejo, S.; Siringan, F.; Thomas, M.A. *Late Quaternary Sedimentation and High-Resolution Sequence Stratigraphy of the East Texas Shelf*; Geological Society: London, UK, 1996.
62. Dalrymple, R.W.; Zaitlin, B.A. High-resolution sequence stratigraphy of a complex, incised valley succession, Cobequid Bay—Salmon River estuary, Bay of Fundy, Canada. *Sedimentology* **1994**, *41*, 1069–1091. [[CrossRef](#)]

63. Gouw, M.J.; Berendsen, H.J. Variability of Channel-Belt Dimensions and the Consequences for Alluvial Architecture: Observations from the Holocene Rhine-Meuse Delta (The Netherlands) and Lower Mississippi Valley (U.S.A.). *Ned. Geogr. Stud.* **2007**, *77*, 124–138. [[CrossRef](#)]
64. Van Wagoner, J.C.; Mitchum, R.M. *Siliciclastic Sequence Stratigraphy in Well Logs, Cores, and Outcrops: Concepts for High-Resolution Correlation of Time and Facies*; The American Association of Petroleum Geologists: Tulsa, Ok, USA, 2003; Volume 234.
65. Wellner, R.W.; Bartek, L.R. The Effect of Sea Level, Climate, and Shelf Physiography on the Development of Incised-Valley Complexes: A Modern Example from the East China Sea. *J. Sediment. Res.* **2003**, *73*, 926–940. [[CrossRef](#)]
66. Willis, B.J. Permeability structure of a compound valley fill in the cretaceous fall river formation of South Dakota. *Am. Assoc. Pet. Geol. Bull.* **1998**, *82*, 206–227.